ISSN 8755-6839

SCIENCE OF **TSUNAMI HAZARDS**

Journal of Tsunami Society International

Volume 31 **Number 2** **2012**

TSUNAMI SOCIETY INTERNATIONAL, 1741 Ala Moana Blvd. #70, Honolulu, HI 96815, USA.

SCIENCE OF TSUNAMI HAZARDS is a CERTIFIED OPEN ACCESS Journal included in the prestigious international academic journal database DOAJ, maintained by the University of Lund in Sweden with the support of the European Union. SCIENCE OF TSUNAMI HAZARDS is also preserved, archived and disseminated by the National Library, The Hague, NETHERLANDS, the Library of Congress, Washington D.C., USA, the Electronic Library of Los Alamos, National Laboratory, New Mexico, USA, the EBSCO Publishing databases and ELSEVIER Publishing in Amsterdam. The vast dissemination gives the journal additional global exposure and readership in 90% of the academic institutions worldwide, including nation-wide access to databases in more than 70 countries.

OBJECTIVE: Tsunami Society International publishes this interdisciplinary journal to increase and disseminate knowledge about tsunamis and their hazards.

Submit manuscripts of research papers, notes or letters to the Editor. If a research paper is accepted for publication the author(s) must submit a scan-ready manuscript, a Doc, TeX or a PDF file in the journal format. Issues of the journal are published electronically in PDF format. There is a minimal publication fee for authors who are members of Tsunami Society International for three years and slightly higher for non-members. Tsunami Society International members are notified by e-mail when a new issue is available. Permission to use figures, tables and brief excerpts from this journal in scientific and educational works is granted provided that the source is acknowledged.

Recent and all past journal issues are available at: http://www.TsunamiSociety.org CD-ROMs of past volumes may be purchased by contacting Tsunami Society International at postmaster@tsunamisociety.org Issues of the journal from 1982 thru 2005 are also available in PDF format at the Los Alamos National Laboratory Library http://epubs.lanl.gov/tsunami/

ISSN 8755-6839

SCIENCE OF **TSUNAMI HAZARDS**

Journal of Tsunami Society International

Volume 31 **Number 2** **2012**

SEA LEVEL SIGNALS CORRECTION FOR THE 2011 TOHOKU TSUNAMI

A. Annunziato[1]

[1] *Joint Research Centre, European Commission*

alessandro.annunziato@jrc.ec.europa.eu

ABSTRACT

The paper analyses the signals measured during the M9.0 Tohoku Tsunami in order to identify the effect of the subsidence on the measurements and to determine correction factors to be applied to the measurements. The objective is to have a coherent set of measurements that can allow the correct estimation of the source term for this event through inversion techniques. In fact the inversion techniques tend to minimize the difference between the measured signals and the calculated value; which means that in the initial period and also for the peak, the solution found without considering this correction tends to get higher values of the source (the peak in some cases is almost 1.4 m higher on a maximum of 4-5 m, thus is not negligible).

The amount of the correction has been determined using the long-term displacement shown in the measurements; the subsidence estimates are also compared with the values obtained using GPS instruments. The analysis shows that the subsidence has a notable influence on the measurements where the deformation is large and that taking into account the deformation in the signals may improve the quality of the estimation of the initial deformation.

Key Words: *Tsunami, Sea Level Measurements, GPS, Tsunami Source, Earth Deformation*

1. INTRODUCTION

A large earthquake occurred off shore the Pacific coast of Tohoku, Japan (38.1035◦N, 142.861◦E, M 9.0 at 5:46:18 UTC on March 11, 2011, that generated a large Tsunami and caused more than 15000 fatalities and more than 4500 missing in the east coast of Japan (Fujii et al, 2011). USGS identified the fault mechanism as dipping trust with strike parallel to the close Japan Trench. The fault movement caused large movements of the earth crust; the continuous measurements of GPS indicated a subsidence of about 1.2 m, close to Central Myagi (Geospatial Information Authority of Japan (GSI)).

The sea level measured during the event is extremely important in order to assess the impact of the Tsunami that has been generated[1]. It is important "during" the event in order to give the Tsunami Warning System operator the information needed to raise or delete an alert of an ongoing event but is also of paramount importance "after" an event in order to estimate the original source of the Tsunami through comparison with focal mechanisms estimations or via inversion methods that use the sea level to find the better combination of source parameters that can explain the observations.

Figure 1 – Identification of several sea level measurements in Japan mentioned in the article

The Japan event is a very important for its dramatic consequences in terms of human lives as well as from the scientific point of view due to the wealth of information available from the large amount of instrumentation present in Japan (e.g. sea level monitoring stations, GPS stations, broadband stations

[1] The sea level datum considered here is the level measured with respect to the mean sea level (MSL) and in general it approximates the Lowest Astronomical Tide.

etc, Figure 1). This instrumentation is able to give the whole picture of the event. This report is aimed at analyzing the response of the Sea Level Instrumentation and to determine if it is necessary to correct some of the measures. In particular the effect of the important subsidence on the measured sea level is not negligible: if on the coast the sea level arrived up to 30-40 m and therefore 1.2 m of subsidence may be negligible, for off shore measurements or tide gauge measurements that shows deviation from their zero in the order of 3-6 m the subsidence plays an important role and may influence the evaluation of the source terms done with the inversion technique. The inversion technique consists in performing a large number of calculations with a fixed fault plane (ex. 50x50 km) and with unitary slip. The comparison with the measured data allows, via least square non-negative solutions (nnls) methods to estimate the contribution of each segment.

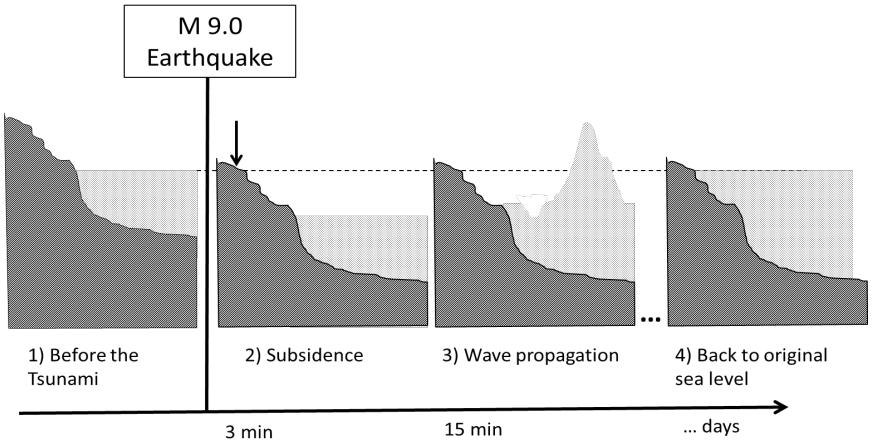

Figure 2 – Sea level response due to the subsidence

2. SEA LEVEL RESPONSE DUE TO THE SUBSIDENCE

Figure 2 shows the sequence of events in case of subsidence. Before the Tsunami (1) the sea level is at a certain elevation dictated by the local tide conditions. At the end of the deformation (estimated in about 3 min for Tohoku Earthquake, USGS), the crust moves downward (2); let's assume the maximum measurement, 1.2 m. As the bottom of the sea also moves, the sea level follows the movement of the crust and thus does not change close to the coastal areas. Far from the coast the deformation may be larger and thus the sea level can be lower than close to the coast. The third phase is characterized by the large wave propagation (3) and is the one that produces damages to the coastal areas. After several hours or days the sea level returns to its original elevation, which does not, depends by the Tsunami and is function of the local tide conditions (4). However since in the meantime the earth crust lowered, there will be parts that were out of the water that now are under the water.

3. SEA LEVEL RESPONSES OF THE VARIOUS INSTRUMENTATION TYPES

The response of the instrumentation to the situation shown above depends strongly on the type of instruments and the measurement method. Three sensors will be considered: the tidal gauges, the floating GPS and the pressure cables or DARTs.

Figure 1 shows the location of the sea level measurements relevant for the Tohoku Earthquake and mentioned in this article. The color indicates the type of device: green or orange dots are tidal gauges, pink dots shows GPS buoys while the blue dots are the bottom pressure cable. It should be noted that the amount and the quality of the instrumentation in Japan has no equivalent on other countries worldwide and allow to analyze in great detail what happened during the 11 March 2011 event.

3.1 Tidal Gauges

The Tidal Gauges are located close to the shore, generally in port areas and consist in a fixed sensor located above the water, connected mechanically with the fixed earth. The sensor (generally microwave) measures the distance between the sensor itself and the water; other types of tidal gauges measure the pressure within a tube connected to the earth and converts it in level. In both cases however the sensor is strictly connected with the earth: any movement of the earth is transmitted to the sensor that thus follows the subsidence.
This means that during the subsidence the measured level may oscillate but after the subsidence it will be very close to the initial one (Figure 3). During the wave propagation or during the return to the original sea level, the sensor may be flooded and can stop working, as occurred in Ofunato (Figure 4). It can be seen by the same figure that the level oscillates after the earthquake but there is not a sharp decrease as it will be evident in the case of the GPS sea level data. After several hours the sea level returns to the original level of tide but the measurement sensor is either destroyed or in any case will show a level greater than the initial level. If the case is the second one the long term level difference between the measured level and the expected tide is a measure of the deformation due to the earthquake.

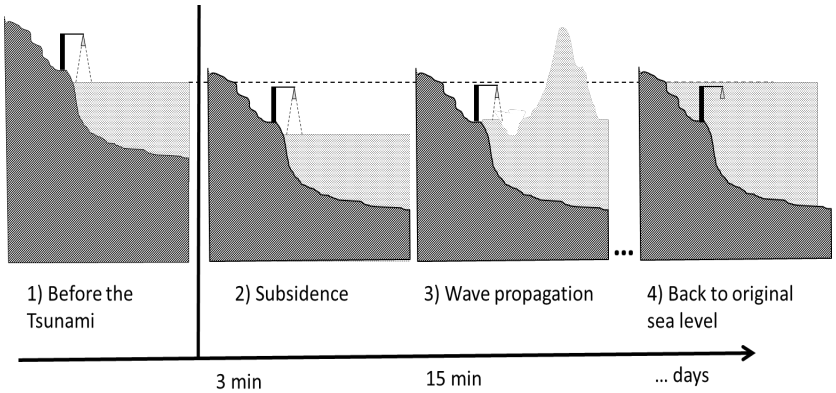

Figure 3 – Sea level response of a tidal gauge

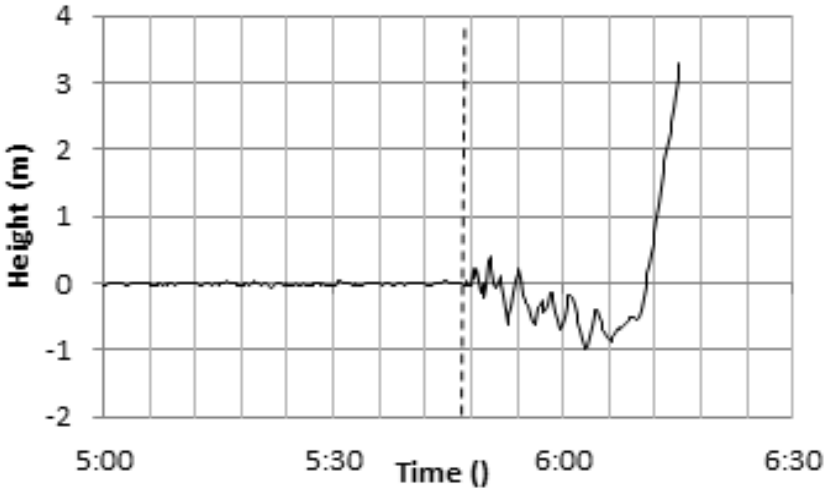

Figure 4 – Sea level measured in Ofunato with tidal gauge

3.2 Floating GPS devices

The floating GPS devices are installed on buoys located about 20 km off shore and measure the geodetic height using satellite navigation systems. However, in order to reduce the error a differential GPS is used: another station, on shore, measures the height and the system performs the difference between these two measured values. Therefore in practical terms the measurement given by the GPS is the height difference between a point on-shore (reference point) and the point where the GPS buoy is installed. The exact position of the reference point is not available for sensitivity reasons. Nevertheless it is located not far from the coast and in line with the location of the buoy[2].
Differently from the tidal gauges, in this case the earth deformation of the reference point could be different from the deformation occurring where the buoy is located because these points are 20-30 km distant each other. As in this case the buoy is closer to the source and this side of the fault is subsiding, it is reasonable to assume that the earth at the location of the buoy will deform more than at the reference point, Figure 5. If this is true the GPS signal will show a sudden decrease at the beginning (as in the case of North Myagi, Figure 6); if the deformation is the same there will be no decrease, as in the case of Fukushima, Figure 8.

In order to get the deformation at the measurement point it is therefore necessary to add 2 contributions: a) the short-term decrease contribution, due to the differential deformation given by different amount of subsidence between the location of the buoy and the location of the reference point; b) the long term offset respect to the normal tide which, as in the case of the tidal gauge, is responsible of the deformation of the reference point (Figure 7 for North Myagi and Figure 9 for Fukushima). The sea level instead has to be reduced, after time 0, only of the long-term contribution, corresponding to the deformation of the reference point.

[2] There is no need to know the precise location of the reference point. This would be useful only to compare the value found with this method with the value obtained by direct GPS measurements on-shore. Wherever is the reference point, the difference in the long term signal is the deformation of the reference point, that needs to be subtracted.

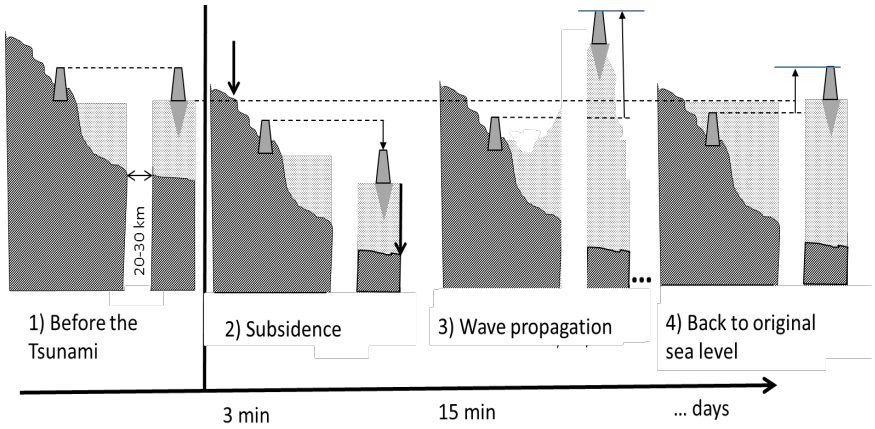

Figure 5 – Sea level response of a GPS buoy gauge

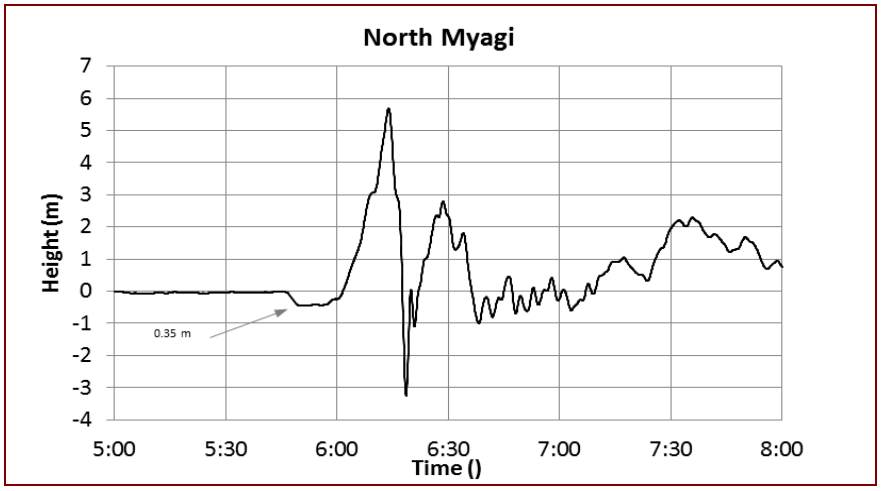

Figure 6 – Sea level measured with GPS buoy in North Myagi where a short term differential deformation of 0.35 m is present indicated with the arrow

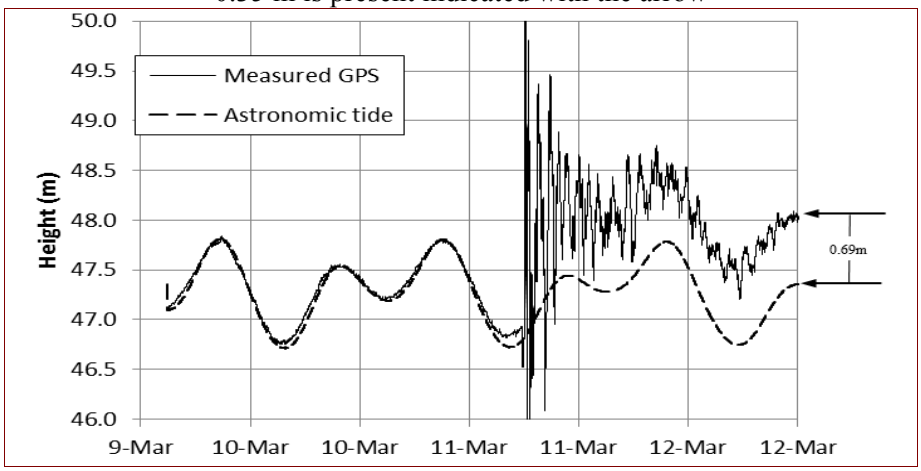

Figure 7 – North Myagi floating GPS: the dash line is the expected tidal sea level while the solid line is the measured level. The offset in the long term is the deformation of the ref. point of -0.69m.

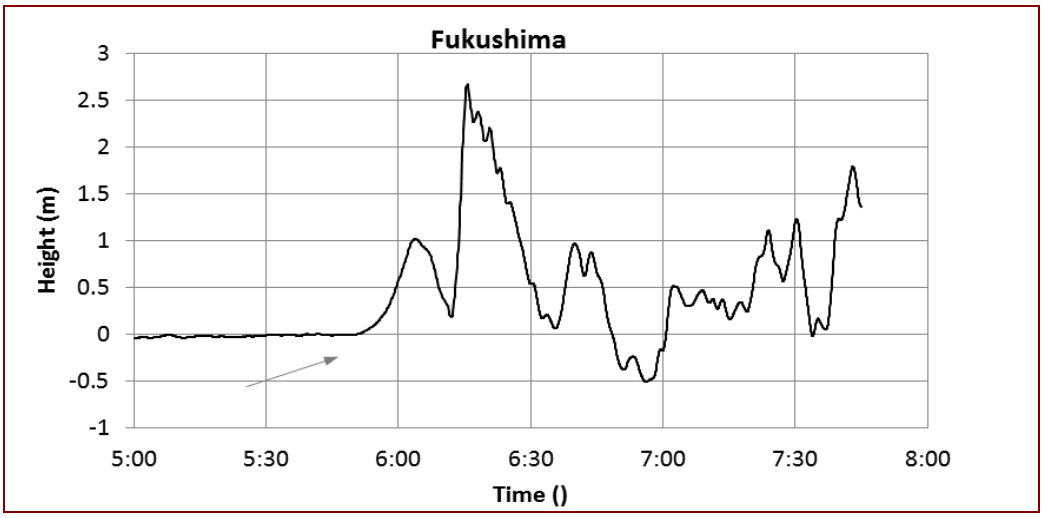

Figure 8 – Short-term sea level measured off shore Fukushima where no differential deformation is present, see the arrow.

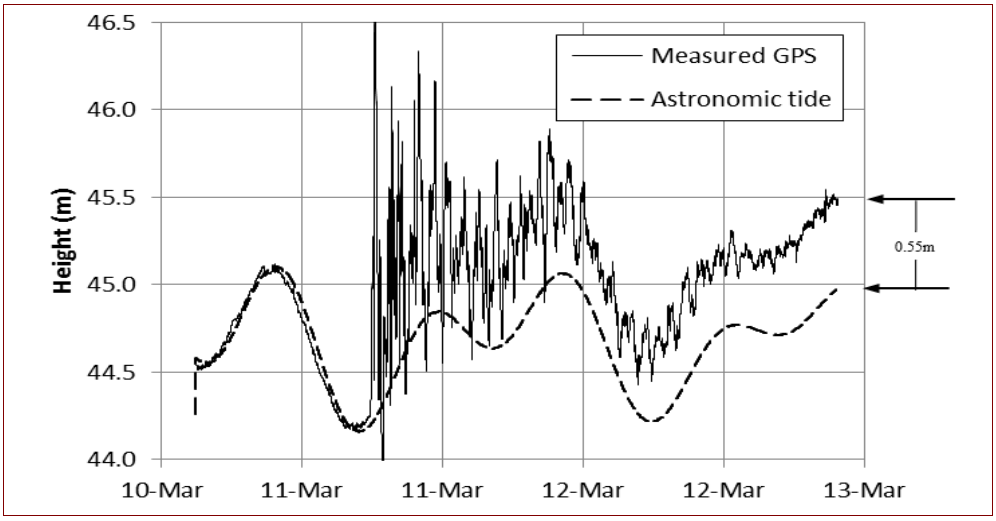

Figure 9 – Fukushima floating GPS: the dash line is the expected tidal sea level while the solid line is the measured level. The offset in the long term is the deformation of the ref. point of -0.55 m

3.3 Deep Pressure Cables or DARTs

The pressure sensors are in a condition similar to both the tidal gauges as well as the GPS sensors. The sensor is located on the bottom of the sea and from its measure it is possible to obtain the level of the water column above it. When the subsidence occurs (Figure 10) the measured level does not change because the deformation and the measurement occurs at the same place. In the long term the difference respect to the value before the Tsunami gives the subsidence level at the location of the

pressure sensor. Figure 11 shows that no decrease is present but only a small oscillation after the earthquake for the cable pressure signals, Maeda et al (2011).

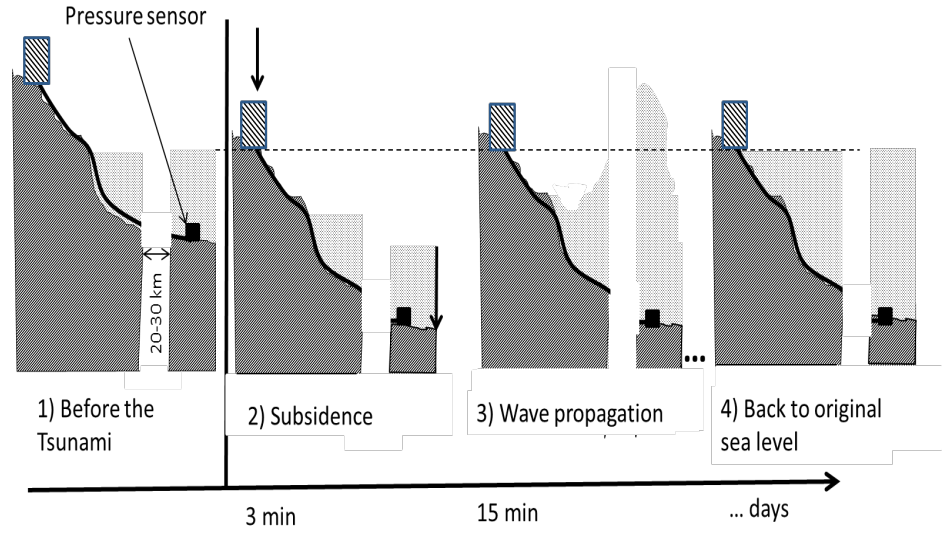

Figure 10 – Sea level response of a cable pressure

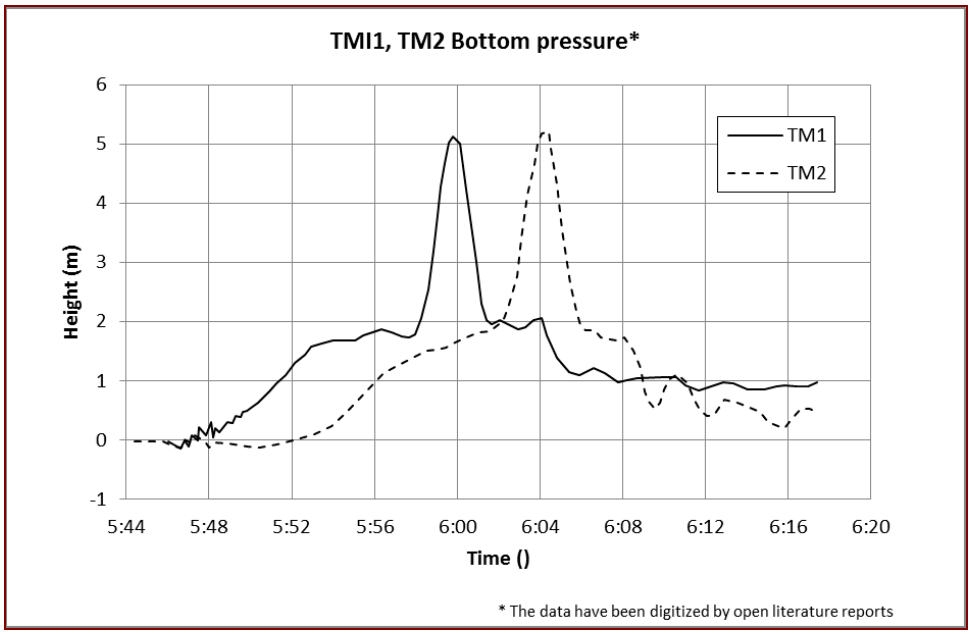

Figure 11 – Original Sea level measured by the cable pressure sensors TM1 and TM2. Long term measurements not yet available

4. SIGNALS CORRECTION FOR THE SEA LEVEL MEASUREMENTS

The analysis of the signals and their explanation indicates that it is necessary to apply a shift to all the measured curves of the devices that in order to take into account the subsidence. Table I shows the different components of the correction (differential deformation or long term offset and its sum).
The values determined are shown in the following Figure 12, which compares also with the value measured with on-shore GPS methods and the agreement is extremely good.
For the points related to TM1 and TM2 where we are not able to determine the deformation due to the absence of the long term data (data unavailable and base station destroyed after the tsunami), an estimate can be done by using the values determined by the Geospatial Information Authority (GSI) using the GPS measurements and correcting by the ratio between measured and estimated from the sea level at the South Iwate GPS buoy. The above offset correction should be applied only after time 0 of the event and within an interval of time between 3 and 5 min; in this analysis it was assumed arbitrarily as 3 min. The original and the resulting curves for 3 examples are shown in Figures 13 to 16. In some cases the correction is small or negligible but in other cases it can be very large. Therefore the comparisons between the calculated values and the measured points should include the corrections indicated above and the inversion methods for the determination of the fault mechanism will also be influenced; in fact up to now, to our knowledge, the correction is not considered and all authors try to match their estimation with the raw data with the tide removed, without any correction.
For instance our code calculations were never able to reproduce the sea level at the pressure cable while instead with this correction and the determined source the agreement is extremely good. The new estimation of the source and the code comparisons will be the subject of another paper.

Lat	Lon	Name	Type	Different. Deform(A)	Ref. Point Def. (B)	Total offset (A+B)	from GPS (GSI)
41.37	141.23	Shimokita	TIDE	0		0	-0.0054
40.12	142.07	North Iwate	GPS	0	-0.15	-0.15	-0.24
39.65	141.98	Miyako	TIDE	0		**-0.5**	-0.36
39.63	142.19	Central Iwate	GPS	0	-0.42	-0.42	-0.55
39.26	142.10	South Iwate	GPS	-0.12	-0.54	-0.66	-0.96
39.25	142.44	TM2	BP	0	n.a.	**-0.96***	-1.4
39.23	142.77	TM1	BP	0	n.a.	**-0.82***	-1.19
39.02	141.75	Ofunato	TIDE	0	-0.7511	-0.7511	-0.82
38.86	141.89	North Miyagi	GPS	-0.35	-0.69	-1.04	-1.27
38.30	141.50	Ayukawa	TIDE	0	n.a	-1.2	-1.19
38.23	141.68	Central Myagi	GPS	-0.34	-1.02	-1.36	-1.51
36.97	**141.19**	**Fukushima**	**GPS**	**0**	**-0.55**	**-0.55**	**-0.78**
36.93	140.90	Onahama	TIDE	0	-0.53	-0.53	-0.57

estimated, not measured

Table I – Correction factors for the sea level measurements

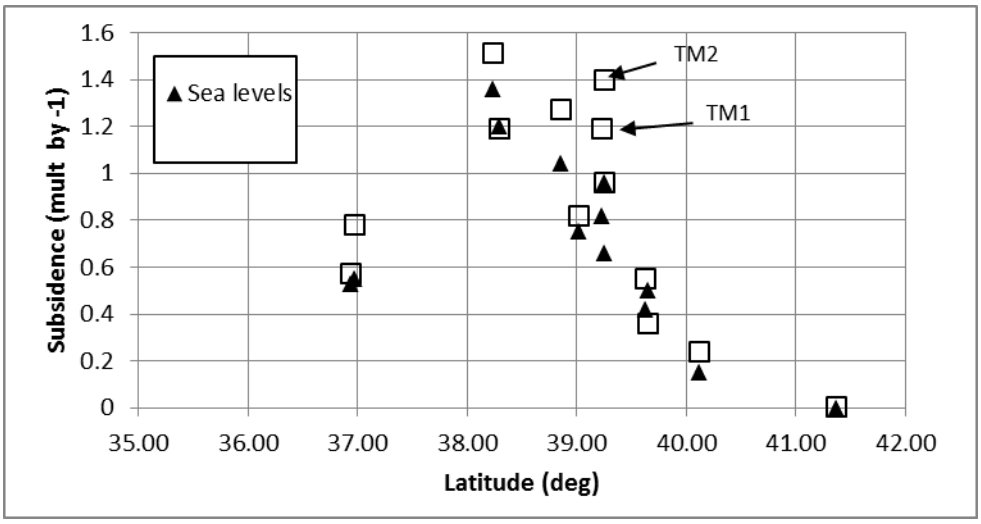

Figure 12 – Comparison of deformations obtained with sea level analysis and direct GPS measurements on land. Some of the points for the level analysis are offshore.

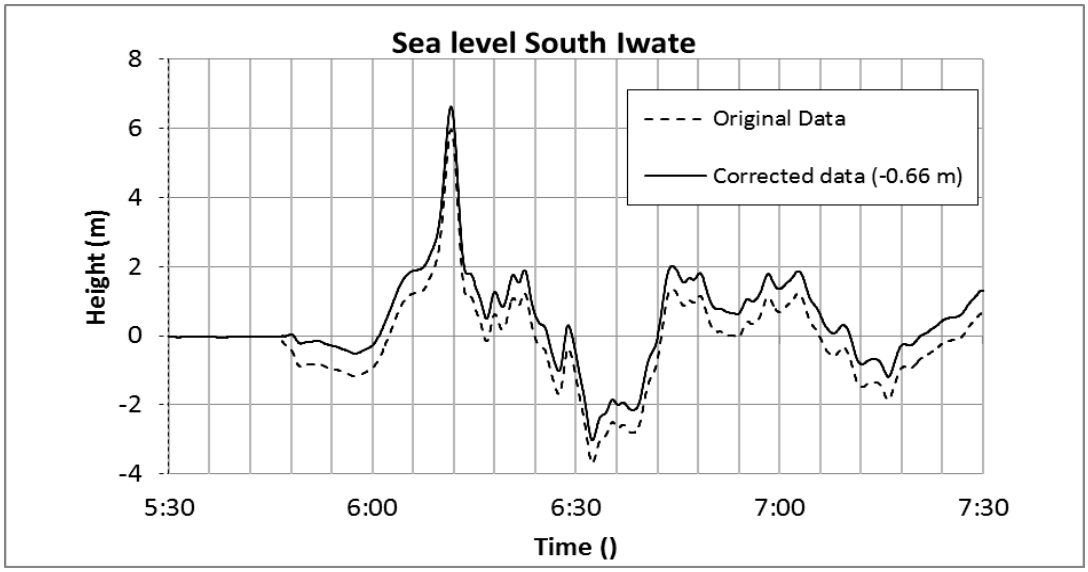

Figure 13 – Original and corrected sea level data for South Iwate

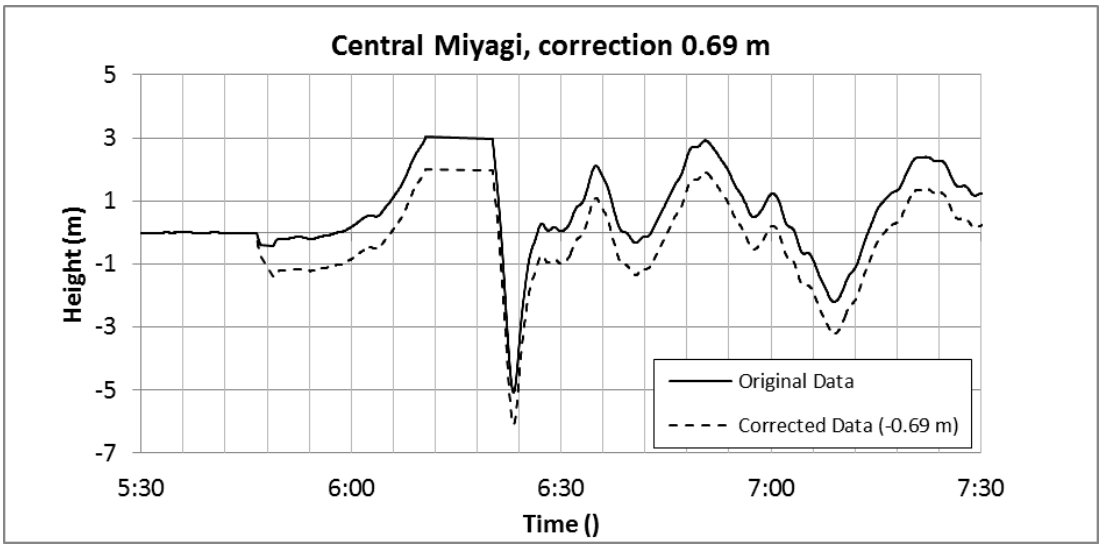

Figure 14 – Original and corrected sea level data for Central Myagi

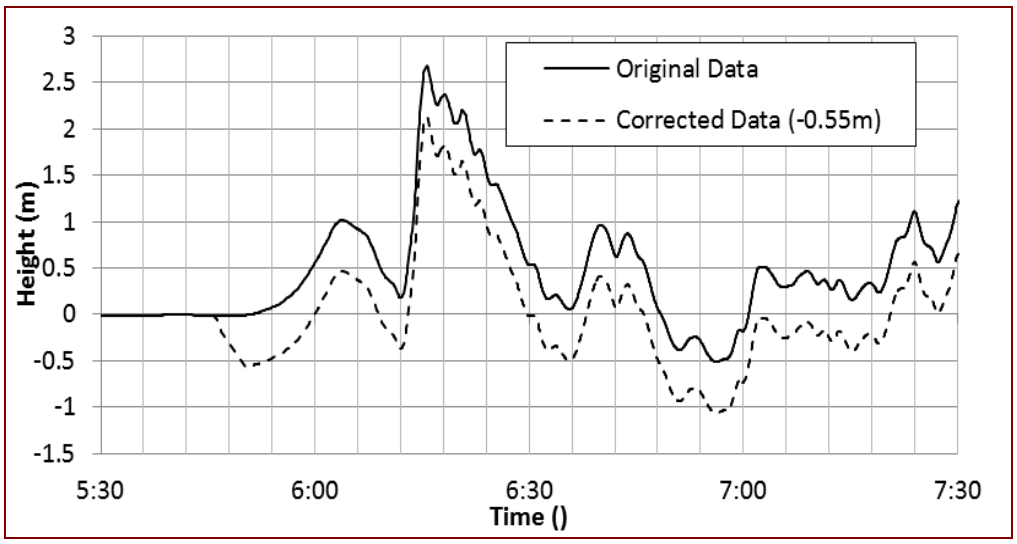

Figure 15 – Original and corrected data for Fukushima

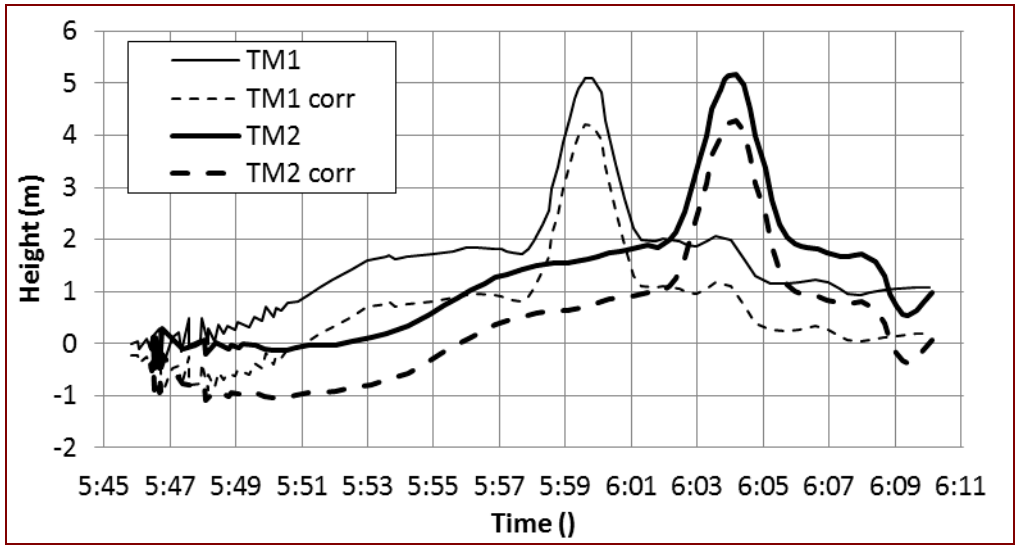

Figure 16 – Original and corrected sea level data for TM1 and TM2, (the data have been digitized by open literature reports)

5. CONCLUSIONS

The analysis of the sea level allowed to estimate the correction factors to be applied in order to take into account the large co seismic subsidence occurred during the Tohoku earthquake. The paper identified 3 different methods of correction for the 3 main types of sea level devices (tidal gauges, GPS buoys and cable pressure or DARTs). It was shown that it is necessary to determine the sea initial level drop and the final sea level offset (differential deformation and long term offset). Through these values it is possible to estimate the initial displacement due to the subsidence.
Although in Japan there is already a large number of on-shore GPS measurements, this paper identified and estimated the subsidence at the location of the GPS buoys and the cable, which are important because in the direction of the fault. It is also possible to estimate the deformation trend along a direction orthogonal to the fault and compare it with the derived source models. Future comparisons with sea level for this event should include the identified correction factors for a proper analysis.

ACKNOWLEDGEMENTS

The author would like to strongly thank the Japan Meteorological Agency and in particular Dr.Takeshi Koizumi. Ports and Harbors Bureau (PHB) under the Ministry of Land, Infrastructure, Transport and Tourism (MLIT) and Port and Airport Research Institute (PARI) provided tide gauge, wave gauge and GPS wave gauge data. GPS deformation data have been provided by Geospatial Information Authority of Japan.

REFERENCES

Y. Fujii, K. Satake, S. Sakai2, M. Shinohara, T. Kanazawa – 'Tsunami source of the 2011 off the Pacific coast of Tohoku Earthquake' – Letter to Earth Planets Space, 63, 815–820, 2011

Geospatial Information Authority of Japan, The 2011 off the Pacific coast of Tohoku Earthquake: Crustal deformation and fault model (preliminary), http://www.gsi.go.jp/cais/topic110313-index-e.html , 2011

U.S. Geological Survey Data
http://earthquake.usgs.gov/earthquakes/eqinthenews/2011/usc0001xgp/#scitech

Tokyo University - Compilation of several information on the 2011 Tsunami - http://outreach.eri.u-tokyo.ac.jp/eqvolc/201103_tohoku/eng/

T. Maeda, T. Furumura, S. Sakai, M. Shinohara – 'Significant tsunami observed at ocean-bottom pressure gauges during the 2011 off the Pacific coast of Tohoku Earthquake' - Earth Planets Space, 63, 803–808, 2011

ISSN 8755-6839

SCIENCE OF **TSUNAMI HAZARDS**

Journal of Tsunami Society International

Volume 31 **Number 2** **2012**

THE INDIAN OCEAN TSUNAMI OF 26 DECEMBER 2004
Analysis of Seismic Source Mechanism

R Mazova[1], B Kisel'man[2], N Baranova[3] and L Lobkovsky[4]

ABSTRACT

Based on the keyboard model of tsunamigenic earthquakes, an analysis was performed of the physical aspects of the 26 December 2004 earthquake off Sumatra and of the seismic source of the great tsunami generated in the Indian Ocean. A simplified keyboard model with vertical displacements of keyboard blocks was used for the numerical simulation in defining the tsunami's generation source and, based on known bathymetry, its subsequent propagation across the Indian Ocean basin. The numerical simulation of the seismic source took into account the oblique character of subduction zone, which was characteristic for this particular earthquake. Furthermore, the analysis evaluated the different scenarios of keyboard blocks motions - corresponding to real seismic and hydro acoustic studies of the earthquake process - as reported in the literature. Adequateness of the calculations performed was verified by comparison of real altimetry records of satellite "Yason-1" with virtual altimetric record, obtained by us for each calculation. The computational analysis helped explain the complex character of the tsunami and of its propagation and energy flux distribution in the Indian Ocean basin.

Key Words: *Indian Ocean tsunami, numerical modeling, satellite altimetry, keyboard model*

[1] Professor, Dept. of Applied Mathematics, N.N. State Technical University, Nizhny Novgorod, Russia 603695
[2] Associate Professor, Dept. of Circuits & Telecommun, N.N. State Tech.Univ., Nizhny Novgorod, Russia, 603695
[3] Magister, Dept. of Applied Mathematics, N.N. State Technical University, Nizhny Novgorod, Russia 603695
[4] Professor, Lab. of Seismology, Institute of Oceanology, Russian Academy of Sciences, Moscow, Russia 117247

1. INTRODUCTION

Special interest was developed in distinguishing the source characteristics of the 26 December 2004 earthquake near Sumatra and of the catastrophic tsunami it generated in the Indian Ocean from other more conventional, tsunamigenic quakes in this region and elsewhere. Two main factors were of particular interest for this event, namely the unusual length of the source region - which extended for nearly 1400 km – and the duration of rupture, which lasted almost 10 minutes. Essentially, such extensive spatial-temporal features of the seismic source complicate the process of using seismographic data in estimating the possible far-field tsunami amplitudes through the use of conventional tsunami numerical simulation methods. The difficulty arises from the fact that seismographs also register reflected signals, which lead to delays in determining the preliminary source parameters with conventional method (Ishii et al. 2005). In contrast to the Pacific Ocean where there are several deep-water pressure sensors, which permit to collect deep-water tsunami amplitude, in the Indian Ocean there was only data from near-coastal tide gauges providing direct measurements of tsunami amplitude and such data often becomes available with considerable delays. Therefore, as one of more effective ways to trace in real time tsunami parameters in the open sea, appears to be through the use of satellite altimetry (Hirata et al. 2006).

The use of altimetric data obtained from satellites "Jason-1" and "Topex-Poseidon" (USA-France) in analysis and numerical simulation of generation and propagation of tsunami (Hirata et al. 2006; Titov et al., 2005) has confirmed that - as expected - parameters of the Indian Ocean 2004 tsunami are determined firstly by details of processes in the seismic source. As known, the process of tsunami formation depends on the character and dynamics of movements in the seismic-source zone, or more definitely, on the initial ocean floor displacements. Knowing the initial stress distribution determines essentially the character of the near-source crustal displacements of the tsunamigenic earthquake source. An earthquake occurs when stress on any part of contact surface overcomes the breaking point and the motion on it is accelerated. This process - depending on earthquake preparation time and initial stress level before seismic movement - will proceed in quite different ways. Tsunami waves generated by such process of vertical displacement will be quite different in each case. This is a fact that must be taken into account in analyzing tsunami mechanisms.

Subduction along the Sunda trench is oblique along the west coast of Sumatra as well as along the Nicobar and Andaman Islands. The slopes of the subduction zone are highly indented, with large segments formed by transcurrent faults passing up to the roof of the subducted plate. Such block structure changes in the subduction zone and permits the use of a keyboard model to deduce the initial seismic source for the purpose of simulating the generation and subsequent propagation of the tsunami (Lobkovsky et al. 2004). The sources of such earthquakes are usually connected with deformation and "shooting" at stress, releasing keyboard blocks with characteristic size near 100 km. Such model with alternative motions of keyboard blocks was successfully applied by this study to simulate the 26 December 2004 Indian Ocean tsunami (Lobkovsky et al. 2006a; Lobkovsky and Mazova, 2007). In particular, a numerical simulation was performed of the 'domino' effect when one of the 'shooting' keyboard blocks near the earthquake epicenter, excites the next keyboard blocks in what corresponds to a uniform character of the rupture motion along the source but with decrease of movement with distance. However, sometimes in the long source several keyboard blocks can be

"shooted" almost simultaneously and this powerful "chord" produces the formation of a huge earthquake source and as a consequence the appearance of giant tsunami (Lobkovsky 1988). Similar multi-block models of the seismic source have been then used by other researchers (Hirata et al. 2006; Ishii et al. 2005; Lay et al. 2005; Song et al. 2005; Wilson 2005).

More detailed numerical simulation was performed by the present study by using a keyboard (multi-block) seismic source located in zone of earthquake 26 December 2004 and generation and the subsequent propagation of the tsunami waves and energy flux distribution in the Indian Ocean basin. To support the analysis, several scenarios of alternative motions of keyboard blocks were used for the extended seismic source and comparisons of tsunami wave heights were performed for given points of the basin, with the results being verified by data obtained by satellite altimetry, by coastal tide gauges and by visual tsunami run-up measurements. Additional verification was also performed by detailed comparison with the results of other studies using the geometry of their model seismic sources.

2. NUMERICAL SIMULATION OF GENERATION OF TSUNAMI WAVES BY SEISMIC SOURCE COMPRISING VARIOUS NUMBERS OF KEYBOARD BLOCKS AND THEIR PROPAGATION

To describe the wave generation and propagation processes a nonlinear system of shallow water equations was used (Lobkovsky et al. 2006b) which for the given case can be presented as

$$\begin{cases} \vec{U}_t + \vec{U} \cdot grad\, \vec{U} + g \cdot grad\, \eta = \vec{F} \\ \eta_t + div\left((H + \eta - B)\vec{U}\right) = B_t \end{cases}$$

where η is the water surface displacement, H is the basin depth, u and v are the components of horizontal wave velocity,

$$\vec{F} = \begin{pmatrix} fv - g\dfrac{u\sqrt{u^2+v^2}}{Ch^2(H+\eta-B)} \\ -fu - g\dfrac{v\sqrt{u^2+v^2}}{Ch^2(H+\eta-B)} \end{pmatrix}, \qquad \vec{U} = \begin{pmatrix} u \\ v \end{pmatrix},$$

where $f = 2\Omega\cos\theta$ is the Coriolis parameter, Ω is the Earth angular velocity, θ is the Earth geographic latitude, g is the gravity acceleration, $Ch = \dfrac{(H+\eta-B)^{0.4}}{sh}$ is the Shezi coefficient, sh is the roughness coefficient, $B(x,y,t)$ describes the basin bottom motion.

To perform the numerical simulation a bathymetric map with one-minute isobath cross-section was used. The calculation region used for the numerical simulations was taken in the geographical square bounded by 10^0 S – 25^0 N, 70^0 – 110^0 E, with grid system that included 1501x 2701 points. By known step on coordinates it was found step on time for the whole basin.

2.1 Main Points of Numerical Simulation

The analysis of numerical simulation scenarios was performed based on results of the following studies (Ammon et al. 2005; Fine et al. 2005; Hirata et al. 2006; Ishii et al. 2005; Lay et al. 2005; Lobkovsky 1988; Nagarajan et al. 2006; Park et al. 2005; Titov et al. 2005). The present analysis used data from tide gauges and from altimetry of the USA-France satellite "Jason-1". As known, almost two hours after the initial earthquake shock, the low-orbit altimetric satellite "Jason-1" scanned the ocean surface for a distance of 1500 km from Sri-Lanka towards the Bay of Bengal. During a time period of 10 minutes, the satellite passed over the tsunami wave front and measured, with accuracy of several centimeters, the ocean surface profile along a 5 km width band along its track (Wilson 2005). The flight trajectory of satellite "Jason-1" is indicated by the white line in Fig. 1a.

In order to adequately evaluate the results of the numerical simulation for each of the chosen scenarios, comparisons were made between the actual data obtained by observations and the virtual altimetric record computed by us for each scenario. Additionally used in the evaluation were the records of functioning tide gauges in the region (Fig.1a) (Nagarajan et al. 2006). Fig. 1b shows the model's seismic source, comprising 13 keyboard blocks.

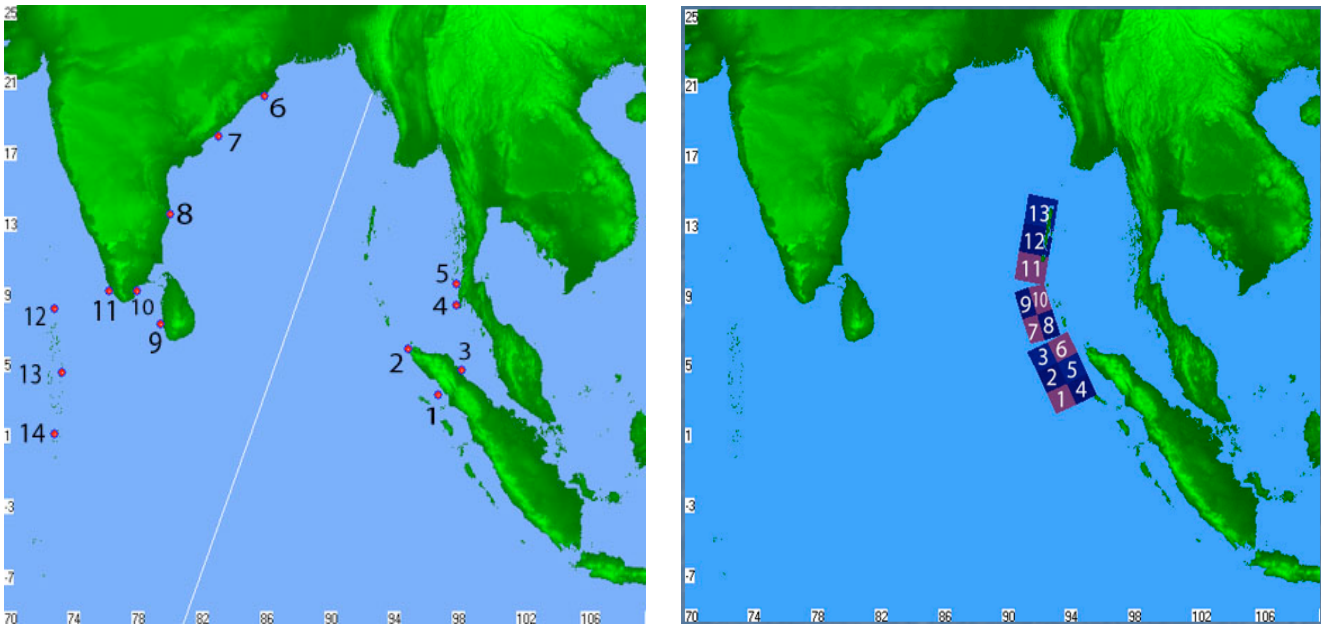

Figures 1a and 1b. Maps of the region impacted by the Indian Ocean tsunami of 26 December 2004. Fig. 1a shows the locations of 14 model recording tide stations and the track of satellite "Jason-1" (white direct line). Fig. 1b shows the 13 keyboard blocks of the seismic source displacements that generated the tsunami. Of these, blocks 1-6 represent the Sumatra segment, 7-10 the Nicobar segment, and blocks 11-13 the Andaman segment.

2.2 Effect of seismic source length to characteristics of propagating tsunami wave and magnitude of wave heights along the coast

For the event of 26 December 2004 there exists an uncertainty in literature with source structure and seismic movements at all length of source. Therefore, it is of interest to study in details the dependence of characteristics of seismic source which generated long surface water wave. (cf. with (Lobkovsky 1988)).

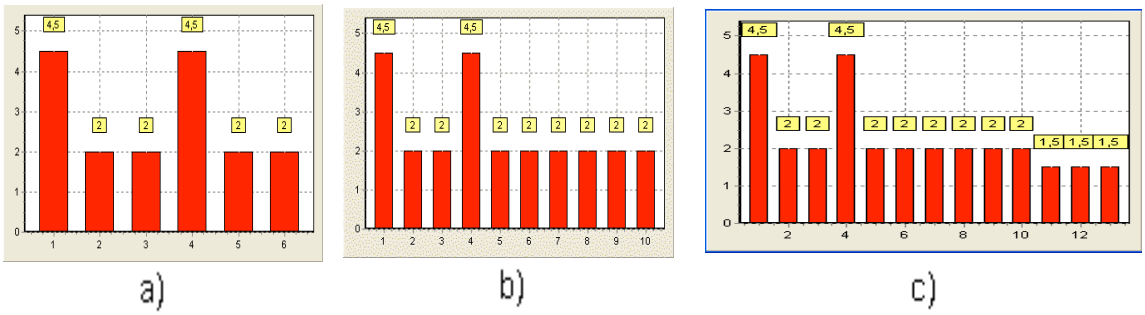

Fig. 2. Schemes of keyboard block uplift used for the numerical simulation: a) Sumatra segment; b) Sumatra and Nicobar segments; c) Sumatra, Nicobar and Andaman segments. The horizontal scale corresponds to the number of keyboard blocks (see Fig.1b), while the vertical scale corresponds to the magnitude of keyboard-block vertical shift (m); figures at the panels correspond to the maximum shift magnitude (in meters).

To accomplish the analysis, consider first the effect of length of underwater seismic source to the development and distribution of the initial tsunami wave field in the basin of the Bay of Bengal and in the central part of Indian Ocean. To analyze further the effect of each large segment of the seismic source that generated the tsunami and the formation of the wave field, it became necessary also to consider three independent contributing sources, namely the Sumatra segment, the Sumatra and Nicobar segments and the Sumatra, Nicobar and Andaman segments (see, Fig. 1b). The magnitudes of maximum keyboard-block displacements for the three seismic source scenarios that were considered are illustrated in Fig. 2. Fig. 3 illustrates the results of tsunami wave generation and propagation for each of these three scenarios. Also shown in this figure is the track and position of the satellite traversing the region (the white line) during this time period.

As shown in Fig. 3a, formed at the ocean surface tsunami source (for the first scenario), generates an almost circular wave pattern, which, due to the bathymetry of the basin, persists in form and propagates faster in a west and southwest direction. Toward the northwest of the Indian coast, the wave arrives with significant delay when compared with the actual recorded wave arrival at tide gauge stations. As seen from the wave field development based on the second scenario (Fig. 3b), the tsunami front becomes more elongated and the time of the first wave arrival on the east coast of India

is decreased - as compared with the case of wave generation only by Sumatra segment (First scenario). When the third segment is included (scenario 3) the wave field is characterized by still more elongated shape to north wave front (Fig. 3c) and the time of the first wave reaching the south-east coast of India is further decreased. It can be seen that along the source side facing the Bay of Bengal, there are three well defined wave fronts corresponding to the designated segments (Fig. 3c). These fronts then form a plane, united front with a subsequent bend in the region of the Nicobar Islands. The change in the character of the wave field for the three cases is well seen from the calculated satellite altimetry shown in Fig. 4.

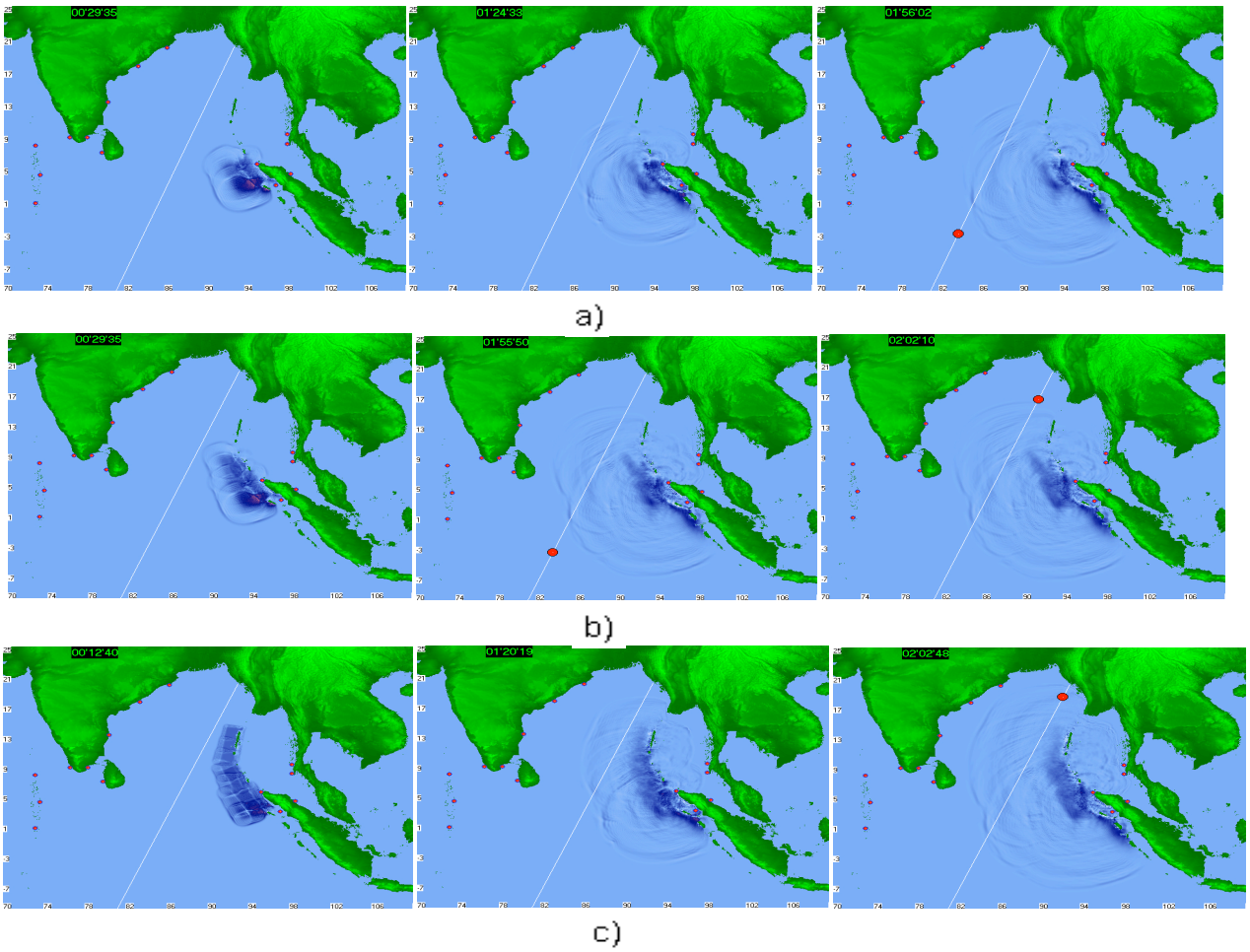

Fig. 3. The generation and propagation of tsunami wave on the Indian Ocean basin: scenario a) - 1; b) - 2; c) - 3. Red point at white line corresponds to the position of virtual satellite in time moment presented at panels

In the calculated picture of the wave field, corresponding to the satellite trajectory (Fig. 1a), some of the observed features appear to be only connected with wave generation by one segment (Fig. 4, upper panel). The characteristic feature is first a positive peak and essentially a larger, negative one.

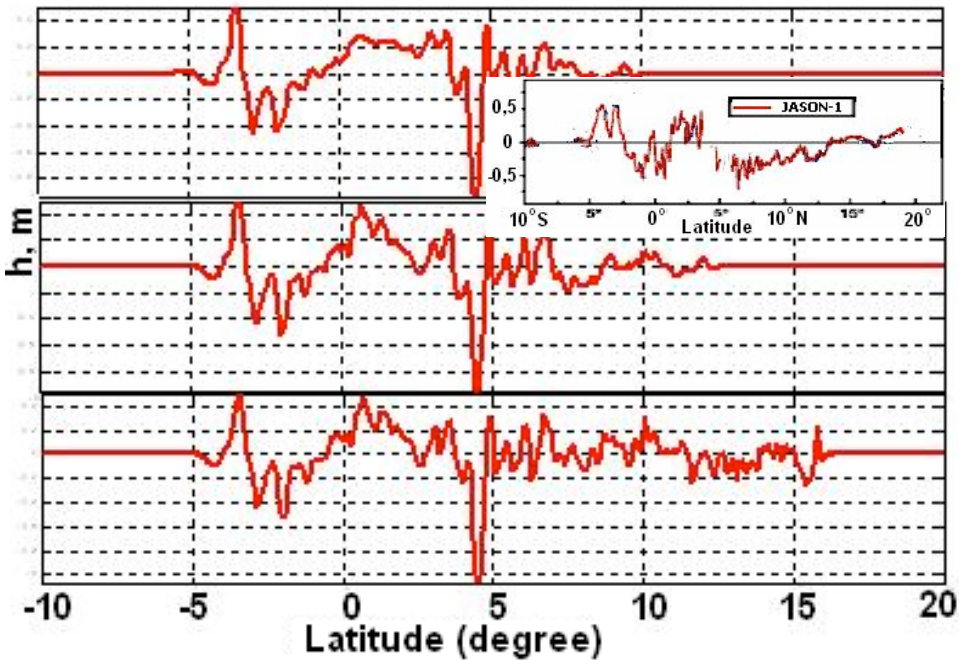

Fig. 4. The virtual satellite altimetry at numerical simulation with scenario 1, 2 and 3 (from up to down). Inset: the real altimetry from satellite "Jason-1".

When the second segment is included, it can be seen that there are changes in satellite altimetry, as a second positive wave is formed and the altimetric record is elongated (Fig.4, middle panel). The inclusion of third segment brings still more changes in altimetric record, although a number of characteristic features of wave fields persist. Therefore, the character of the leading wave, its height and its propagation in all three cases remain unchanged. However, it should be noted that there is a rise in the wave level behind the two negative peaks that are formed and that their amplitude is larger when compared with those exhibited with scenarios 1 and 2 (upper and middle panels). The characteristic negative peak, appearing already for scenario with only the Sumatra segment, is observed in all three calculations. However, in the third calculation its amplitude somewhat increases(lower panel). Also, it is well observed that with increasing of source length the satellite altimetric record is elongated and in the third case satellite fixes wave up to the moment of its passing the basin and its disappearance over the area. Thus, the wave field picture is in greater agreement with the results of satellite altimetric observations in both the region of the leading wave and, essentially, in the latitude region corresponding to the Nicobar Islands (Lay et al. 2005). Thus, the inclusion of the calculations of the second and third segments of the underwater seismic source, has no noticeable effect to leading wave, however, there appear significant changes in wave characteristics in the vicinity of the Nicobar and Andaman Islands as well as along the impacted coasts corresponding to these segments. As seen in Fig. 4 (lower panel), the calculated wave field picture corresponding to satellite trajectory is close to the observed altimetry of satellite "Jason-1" (see inset at Fig.4).

2.3 Numerical simulation of tsunami wave generation by seismic source comprising various numbers of keyboard blocks and subsequent wave propagation

To realize scenario 4, considered was a seismic source comprising 14 keyboard blocks and extending for 1400 km along the Sumatra-Nicobar-Andaman deep-sea trench. The keyboard blocks were 100 km long and 150 km wide. Their coordinates and sizes of the blocks were taken from the literature (Hirata et al. 2006), where such source was based on satellite data of sea surface height profiles and ocean floor rupture and deformation propagating to the north from Sumatra Island with very low velocity - less than 1 km/sec (in average). The scheme of movements of keyboard blocks for this scenario is presented in Table 1.

Table 1. Parameters of keyboard block movements for scenario 4

Block number	1	2	3	4	5	6	7	8	9	10	11	12	13	14
Shift value (m)	9	8	6	6	4	4	2	2	2	2	2	1,5	1,5	1,5
Shift time (Sec)	30	60	90	120	150	180	210	240	300	360	420	480	540	600

Shown in the second row of this Table are the maximum values of vertical shift for each of the keyboard blocks of the seismic source. Shown in the third line is the time of movement of each keyboard block. From the above Table, it can be seen that each keyboard block begins to move after the motion of the preceding block terminates. Also shown is that the first 8 blocks lift up to maximum height for about 30 seconds, but all subsequent blocks for 60 seconds. The total time of motion from south to north is 600 sec (10 min). Presented in Figure 5 below are six time steps during tsunami wave generation by the seismic source, comprising 14 keyboard blocks and moving sequentially from south to north. In two last figures the fixed positions of satellite "Jason-1" can be seen as it moves along its trajectory

The picture of maximum wave height distribution obtained from this simulation, demonstrates that the highest wave height was observed along Sumatra, the Indian coast, Sri-Lanka, the Maldives and along numerous other coastlines. – Qualitatively this is in good agreement with the actual observations and recordings of the event. Our preliminary analysis demonstrated that the vertical components of keyboard block shifts cannot exceed 9 meters since larger maximum uplift of keyboard blocks results in significantly larger vertical shifts of the free water surface in the Indian Ocean than those determined with the data from satellite "Jason-1". So, the given scenario at which rupture is directed successively from south to north and vertical shift reaches significant magnitudes (see above), obviously is not optimal.

On the basis of analysis of seismic and hydroacoustic data given in the literature (Ammon et al. 2005; Borges et al. 2005; Guilbert et al. 2005; Hirata et al. 2006; Ishii et al. 2005; Lay et al. 2005; Nagarajan et al. 2006; Park et al. 2005; Song et al. 2005; Titov et al. 2005; Park et al. 2005) different

scenarios were considered where the movement of the keyboard blocks in the seismic source was not only successive from south to north with various orientation of movements and different speeds, but was also alternating. Evaluation was performed of results of virtual satellite altimetry, obtained by us for each calculation.

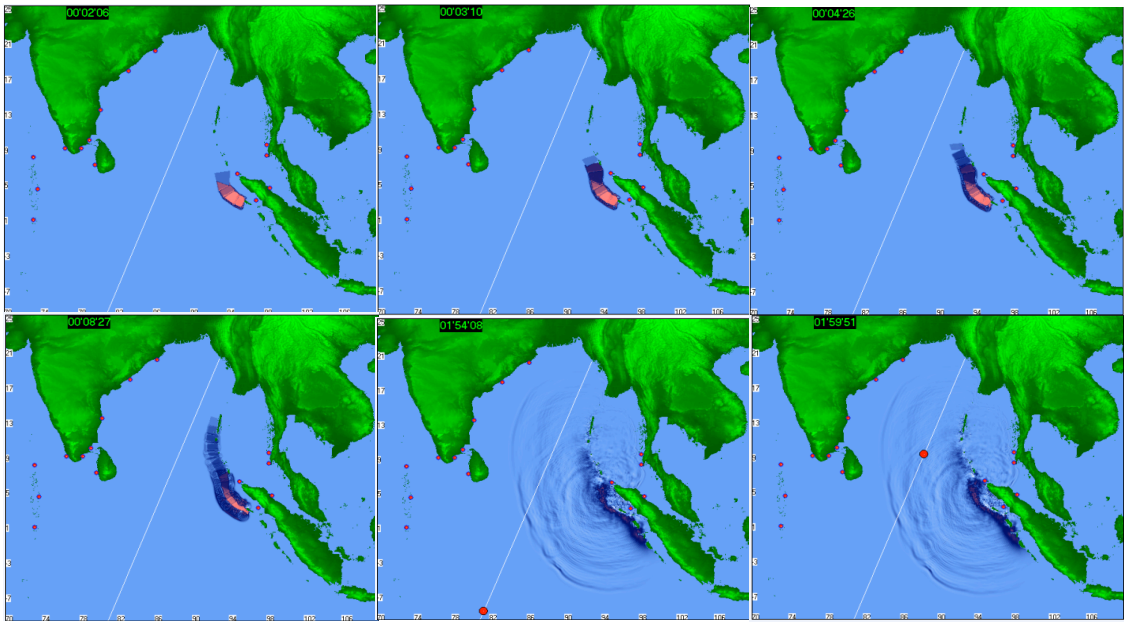

Fig. 5. Scenario 4. Tsunami wave generation from seismic source comprising 14 keyboard blocks.

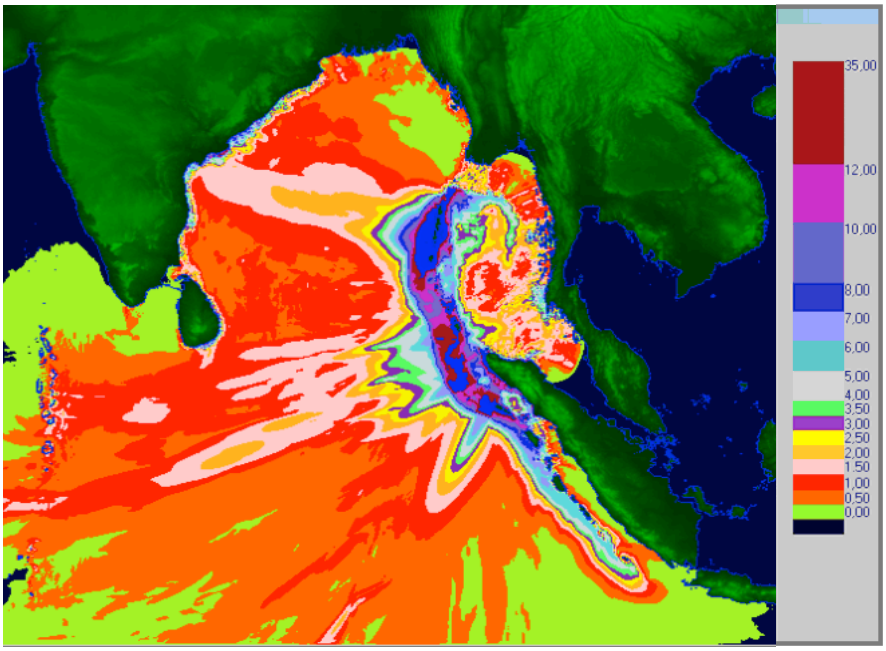

Fig. 6. Distribution of maximum tsunami wave height for scenario 4.

Shown in Figure 7 are three variants of the simulation: the upper panel corresponds to scenario 4, the middle one to scenario 5 and the lower one to scenario 6.

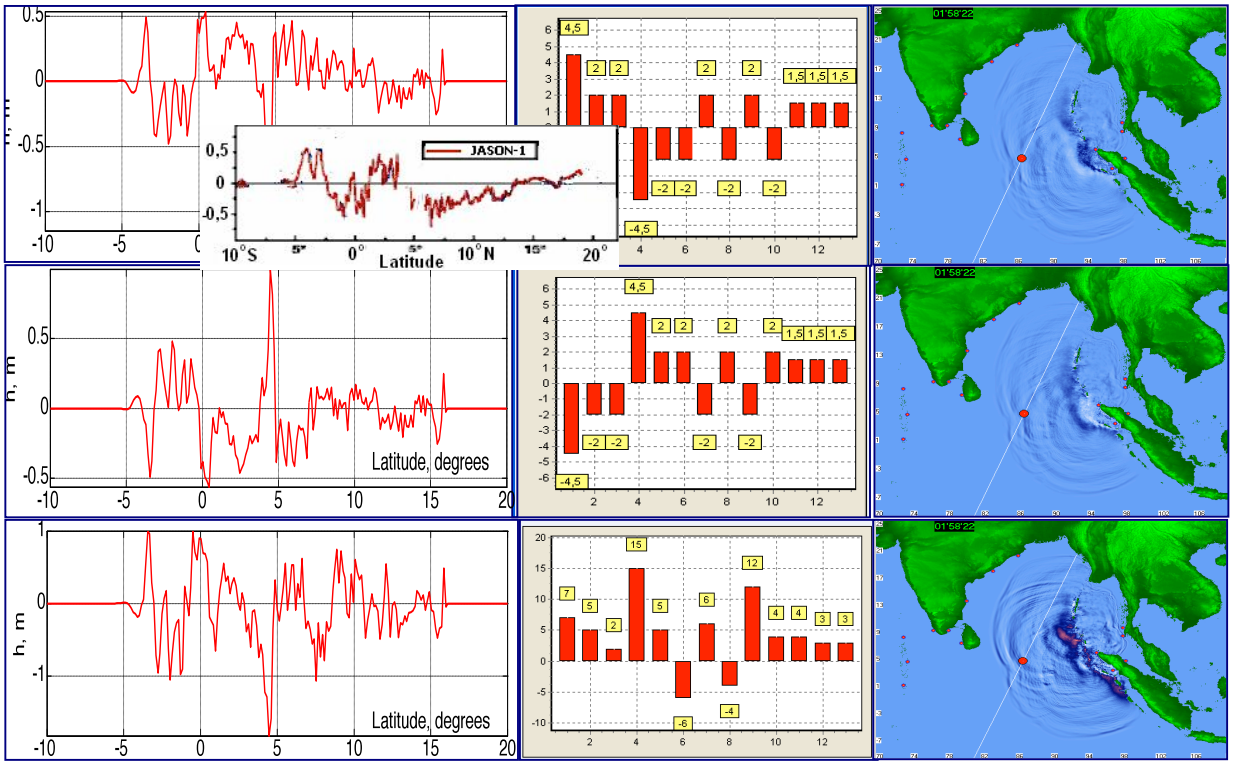

a) b) c)

Fig. 7. The results of numerical simulation with scenarios 5-7: a) virtual satellite altimetry with scenarios 5-7; b) sketch of location of keyboard blocks in seismic source; c) wave field distribution for each scenario; white direct line corresponds to the flight trajectory of satellite "Jason-1" and red dots on this line correspond to the position of satellite at given moment of time.

In Fig.7a presented are the results of model altimetric record at simulation of motion of virtual satellite along trajectory of real satellite "Jason-1". Shown in Figure 7b is a schematic view of the moment of maximum uplift of keyboard blocks. Figure 7c illustrates the calculated picture of wave field distribution and the position of the virtual satellite two hours and forty minutes after the main earthquake. According to scenarios 5-7, the seismic source - comprising three segments (see Fig. 1b) - is subdivided to the following blocks: the first segment is that of Sumatra (blocks 1-6), the second is that of the Nicobar Islands (blocks 7-10) and the third is that of the Andaman Islands (blocks 11-13). For scenario 5 the keyboard blocks with negative displacement (4, 5, 6, 8, 10) are oriented towards the Island of Sumatra and, in contrast to scenario 4, differ in vertical movement magnitude and in the sequence of keyboard block lifting. Scenario 6 is symmetrical to scenario 5, the motion of keyboard blocks being oriented downward towards the ocean (1-3, 7, 9), but the rest of the blocks move upward. To perform more adequate estimations, the magnitudes of maximum shifts of

keyboard blocks used for scenarios 5 and 6 were the same. For scenario 7, keyboard block displacement reached 15 m. Keyboard blocks with negative displacements (6 and 8) are oriented towards Sumatra (see, Table 2) but the motion of keyboard blocks begins from keyboard block 4 (see Table 2). As expected, the satellite altimetry of wave heights for both scenarios 5 and 6 is 'inverted'. However, for scenario 7, the wave train following the leading wave is characterized with large positive peaks. The significant negative tails, appearing behind the central positive part of the signal at the lifting of the first keyboard blocks up, are characteristic for scenarios 5 and 7.

Table 2**.** Parameters of keyboard block movements for scenario **7**

Block number	1	2	3	4	5	6	7	8	9	10	11	12	13
Shift value (m)	7	5	2	15	5	-6	6	-4	12	4	4	3	3
Start time (sec)	30	30	60	0	30	60	120	120	240	240	360	440	520
Stop time (sec)	120	60	180	30	240	300	300	360	360	360	480	480	600

For scenario 6, the altimetry obtained is qualitatively different of the real altimetry, which indicates the impossibility of such a scenario - where part of the seismic source facing the ocean is associated with negative movement. For scenarios 5 and 7, the change in the extent of displacements of the first keyboard blocks affects the behavior in the central part of the graphics - which in both cases can be explained by resonance effects at interaction of wave fronts coming from different segments. The picture of the wave field computed for scenario 5 is presented in Figure 8 where 9 time moments of tsunami generation and propagation from the seismic source are presented. It is well seen that the forming tsunami source (upper panels), is dipolar in character. Indeed, closer to the Island of Sumatra a depression is observed while on the open ocean side from the source an elevation of water surface is formed.

With increasing time, negative waves reached the coast of Sumatra, leading to a withdrawal of the water from the shore – which was indeed observed. However, the whole wave field character in the open ocean is consistent with the results of other studies. The computed frontal profile of sea surface height, during the passing of the tsunami wave, corresponded to the time and path trajectory of the satellite and the measurements in this scenario are essentially closer to the satellite data - as they relate to both the leading wave and the characteristic sharp depression of the ocean surface as determined by the satellite during its passage near the Nicobar Islands. This permits to suggest that such a scenario is closer to reality of the given structure of movements of the seismic source. However, it is necessary to note that satellite altimetry obtained in its tail part is somewhat different from the real record. In real altimetry the curve of the profile of sea surface height along the satellite's trajectory is located below the abscissa axis, which in fact indicates that for large part of its flight path, the satellite determined the depression of water level in the ocean.

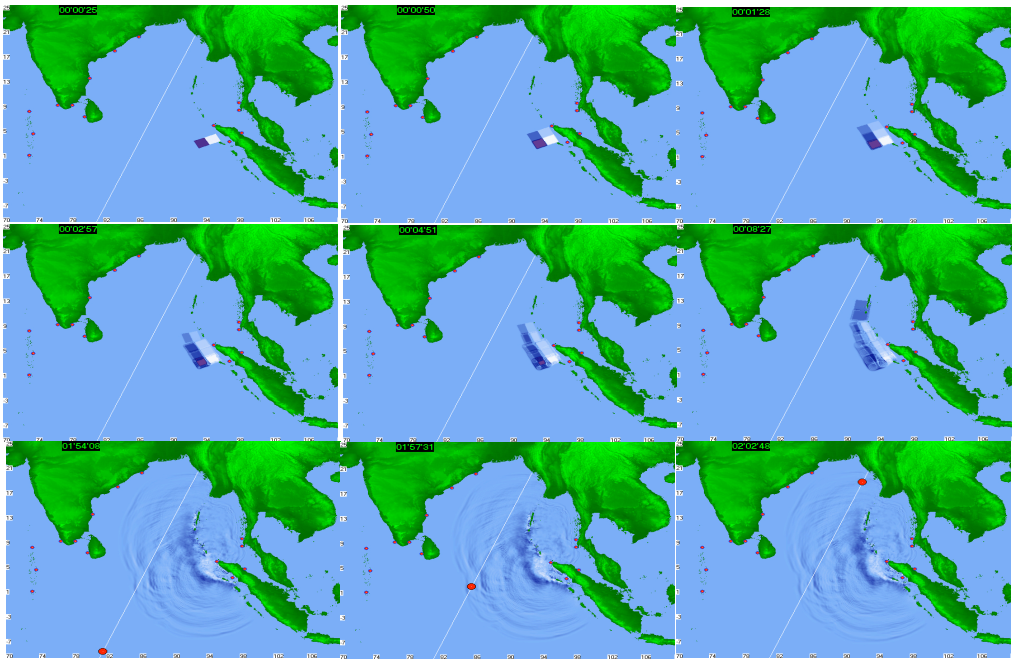

Fig. 8. Formation of tsunami source and propagation of tsunami wave in the Indian Ocean basin for scenario 5. At lower three panels; there are fixed time moments of the flight of the virtual satellite.

To approximate the character of the computed curve to the natural one, a numerical simulation was performed on scenario 8, which differs from those of scenarios 5 and 7 in the order of motion of some keyboard blocks. In scenarios 7 and 8, the setting of keyboard motions in the earthquake source approximated the results of other work (Ishii et al. 2005) (see, Table. 2 and 3) and is in the following order: $4 \rightarrow 2$, $1 \rightarrow 3 \rightarrow 5 \rightarrow 6$, $7 \rightarrow 8$, $9 \rightarrow 10 \rightarrow 11 \rightarrow 12 \rightarrow 13$.

Table 3. Parameters of keyboard block movements for scenario 8

Block number	1	2	3	4	5	6	7	8	9	10	11	12	13
Shift value (m)	4,5	2	2	-4,5	-2	-2	2	-2	2	-2	1,5	1,5	1,5
Start time (sec)	30	30	60	0	120	180	180	240	240	300	360	420	480
Stop time (sec)	120	60	180	30	240	300	300	360	360	360	480	480	600

The values of shifts are set somewhat less than for scenario 7 since the altimetric record of the satellite at simulation of scenario 7 results in essentially excessive magnitudes of sea surface height (see Fig. 7, lower panel). For scenario 8 the magnitudes of height in the altimetric record are closer to the real data (Figure 9).

Furthermore, the magnitude of the negative peak is decreased and the curve of sea surface height profile is located below the zero level - which corresponds better to the real altimetric record from satellite "Jason-1" as compared with the simulation on scenarios 5 and 7. Thus, a tendency of the source formation of the 26 December 2004 earthquake becomes better defined. A sequence of multi-block movements occurs along the source with the normal fault oriented towards Sumatra Island, while strong reverse fault is oriented on the ocean along the Sumatra segment of the source. The Nicobar segment of source normal fault is oriented towards Thailand and a reverse fault, somewhat weaker as compared with the Sumatra segment, is also oriented towards ocean. Thus, keyboard motion is not strictly successive from south to north.

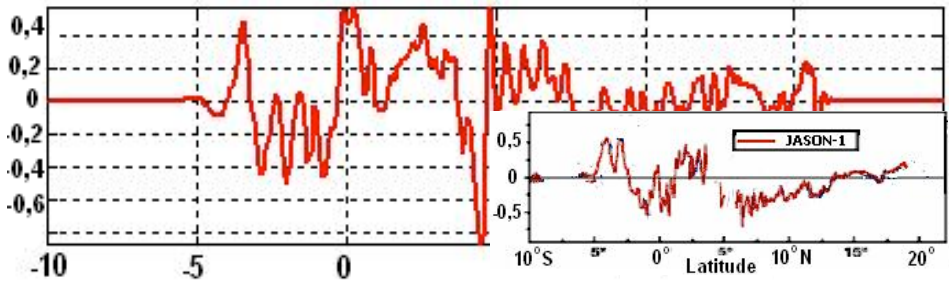

Fig. 9. The virtual satellite altimetry for scenario 8.

2.4 Spectral analysis of results of the numerical simulation of tsunami waves

The data about the change of surface water height obtained by satellite facilities were used to estimate spectral characteristics of tsunami waves in the open ocean, propagating towards India and Sri-Lanka. Using the above stated results, wavelet-analysis and comparison with spectrogram were performed with the available altimetry data of satellite "Yason-1" (Kulikov et al. 2005).

A spectral analysis of computed altimetry is shown in Figure 10 obtained for scenarios 4 and 7. Figure 11 illustrates the wavelet analysis for scenarios 1-3, which permits to estimate the influence of the length of seismic source to the wave characteristics of the tsunami in the open ocean with the use of computed satellite altimetry. From this, it becomes obvious that when the seismic source comprises only one segment (Sumatran one) (upper panel), then the low-frequency component is well localized in the interval ranging from 3S to 7N and is of significant intensity. This region corresponds to a wavelength of the order of 500 km. Around this region there are three, well defined zones of intensity (black and black-grey ovals). Upwards, black-grey regions occur with two characteristic peaks in regions of higher frequencies. When the second segment (Nicobar one) is included (middle panel), the low-frequency area is somewhat smoothed and becomes less intensive. However, there are significant distortions in the right part of spectrum, in the interval ranging from 5N to 10N, in the wavelength range of the order of 200 km. The low-frequency part of the spectrum is shifted to 15N. When the third segment (Andaman one) is included, the intensive low-frequency area is elongated to 7 N, while the less intensive area occurs at 15N. The next expressed frequency area is almost the same as in the case of the two segments and the frequency area at the level of 10^{-2} becomes more intensive.

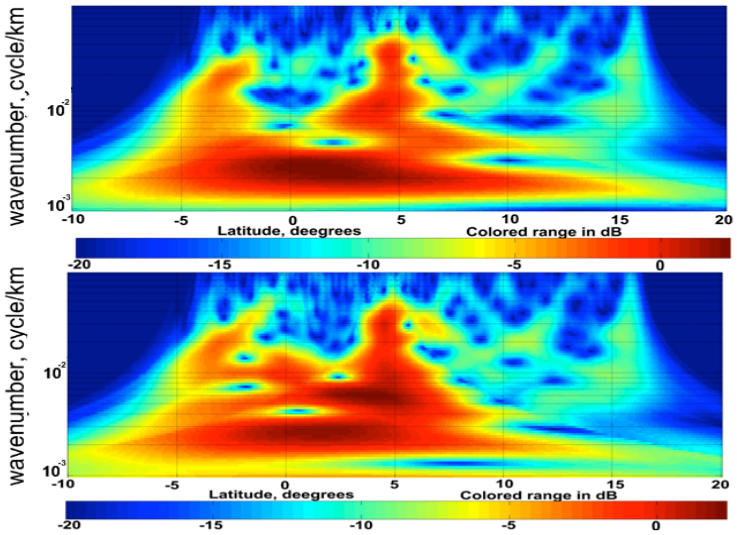

Fig. 10**.** Wavelet-analysis for altimetry, obtained at realization of scenarios 4 and 7.

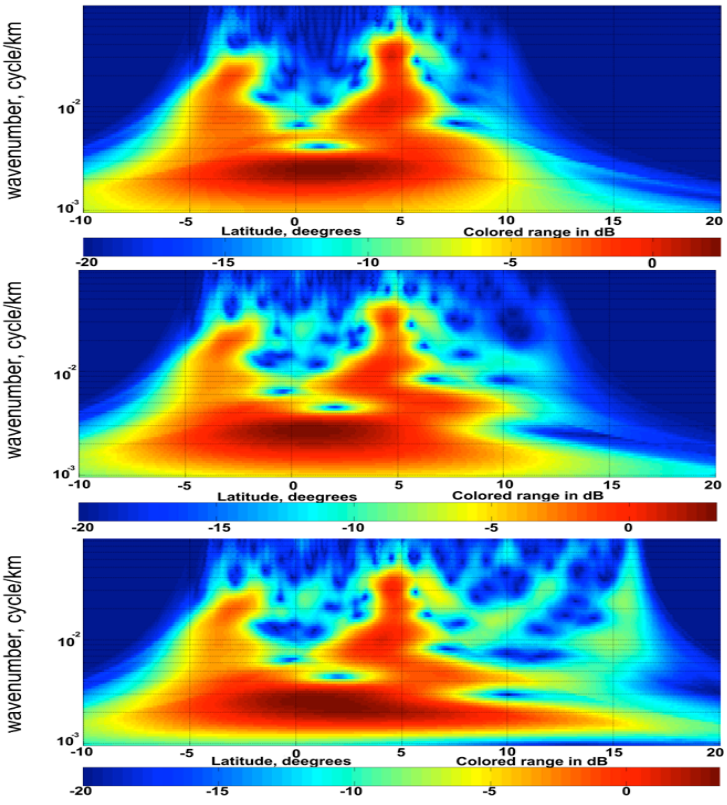

Fig.11.Wavelet-analysis for altimetry, obtained by analysis of influence of the length of the seismic source: upper panel – 1 segment; middle panel – 2 segments; lower panel – 3 segments (for more details, see the text).

It should be noted that for all three cases the left part of the spectrogram remained practically unchanged. It is well seen that low frequencies enter the region earlier than higher ones, which permits to conclude that it is consistent with findings (Kulikov et al. 2005) about the presence of high-frequency dispersion. In the spectrogram there are well-seen "large" and "small" hills coming on horizontals 0.02 and 0.05-0.06, respectively. It is also seen that a delay with the appearance of harmonic components increases with their wave numbers. The results of the present analysis demonstrate the importance of the effect of linear dispersion on the propagation and transformation of tsunami waves in the Indian Ocean and the necessity of taking into account this effect at numerically simulating tsunami wave propagation.

3. DISCUSSION AND CONCLUSION

The results of the numerical simulation demonstrate that by using the keyboard structure of an underwater earthquake source and by changing its dynamics, it is possible to obtain essentially a different wave field character for surface wave generation. With such a process of tsunami source formation, the magnitudes of maximum wave heights and their distribution on the shore can be determined. The estimations of wave height at 10 m isobate, even in a simplified model, give the opportunity to select the seismic source configuration. By using a simplified keyboard model and by taking into account the vertical components of keyboard block displacement of the seismic source, we were able to select the most possible kinematical process describing adequately the tsunami's wave field behavior in Indian Ocean basin for the given tsunami. It should be also noted that the motion of the keyboard blocks in the seismic source region is not successive from south to north and that the present analysis is consistent with results of numerous other studies. Furthermore, the use of different scenarios of kinematic motions of keyboard blocks in the seismic source region used in the present study, permitted the determination of the optimal source parameters that were responsible for tsunami generation and to conclude what the best-fit source was. It also helped illustrate that the most adequate formation of the earthquake source responsible for the tsunami was when the normal fault is oriented towards the Island of Sumatra and the strong reverse fault occurred towards the ocean side of the Sumatra segment of the source, while in the Nicobar segment of the source, the normal fault is oriented towards Thailand, but with somewhat weaker reverse fault than that along the Sumatra segment oriented towards the open ocean. It is necessary also to note that using of wavelet analysis of altimetric records of virtual satellite flights for each scenario permitted the confirmation of our suggestion on the probability of realization of such scenario.

Acknowledgments

The present study was supported by the Russian Foundation for Basic Research, project no. 12-05-00808.

The authors appreciate Dr. George Pararas-Carayannis' critical reading and careful editing.

REFERENCES

Ammon C.J., C.Ji, H.-K. Thio, D.Robinson, S.Ni, V.Hjorleifsdottir et al., 2005. Rupture Process of the Great Sumatra-Andaman Earthquake // *Science* 308, 1133-1139.

Borges J.F., Caldeira B., and M.Bezzeghoud, 2005. Source rupture process of the great Sumatra, Indonesia earthquake (M_w=8.9) of 26 December 2004 (Preliminary Results), *unpublished*) 1-6.

De Groot-Hedlin C.D., 2005. Estimation of the rupture length and velocity of the great Sumatra earthquake of Dec 26, 2004 using hydroacoustic signals, *Geophysical Research Letters* 32, L11303 (1-4).

Guilbert J., Verzog J., Schissele E., Roueff A., and Y.Cansi, 2005. Use of hydroacoustic and seismic arrays to observe rupture propagation and source extent of the M = 9.0 Sumatra earthquake, *Geophysical Research Letters* 32, L15310 (1-5).

Hirata K., Satake K., Tanioka Y., Kuragano T., Hasegawa Y., Hayashi Y., and N. Hamada, 2006. The 2004 Indian Ocean tsunami: tsunami source model from satellite altimetry, *Earth Planets Space* 58(3), 195-201.

Ishii M., Shearer P.M., Houston H., and J.E.Vidale, 2005. Extent, duration and speed of the 2004 Sumatra-Andaman earthquake imaged by the Hi-Net Array, *Nature* 435, 933-936.

Lay T., Kanamori H., Ammon C.J., Nettless M., Ward S.N., Aster R.C., et al., 2005. The Great Sumatra-Andaman Earthquake of 26 December 2004, *Science* 308, 1127-1133.

Lobkovsky L.I., 1988 *Geodynamics of spreading and subduction zones, and two-level plate tectonics* (Moscow, Nauka Press).

Lobkovsky L.I., Nikishin A.M., and V.T.Khain, 2004. *Current problems of geotectonics and geodynamics* (Moscow, Scientific World).

Lobkovsky, L. I., R. Kh. Mazova, I. A. Garagash, L. Yu. Kataeva, and I. Nardin 2006a To analysis of source mechanism of the 26 December 2004 Indian Ocean tsunami, *Russ. J. Earth Sci.*, V.8, ES5001, doi:10.2205/2006ES000208.2006 http://dx.doi.org/10.2205/2006ES000208,

Lobkovsky L.I., Mazova R.Kh., Kataeva L.Yu., and B.V.Baranov, 2006b. Generation and propagation of catastrophic tsunami in the Sea of Okhotsk basin. Possible scenarios, *Doklady RAS* 410, 528-531.

Lobkovsky L.I., and R.Kh.Mazova, 2007. Source mechanism of the tsunami of 2004 in the Indian Ocean: analysis and numerical simulation, Izvestiya. Physics of the Solid Earth 43, 573- 582.

Nagarajan B., Suresh I., Sundar D., Sharma R., Lal A.K., Neetu S., et al., 2006. The Great Tsunami of 26 December 2004: A description based on tide-gauge data from the Indian subcontinent and surrounding areas, *Earth Planets Space*, 58, 211–215.

Park J., Song T.-R.A., Tromp J., Okal E., Stein S., Roult G., et al., 2005. Earth's free oscillations excited by the 26 December 2004 Sumatra-Andaman earthquake, *Science* 308, 1139-1146.

Song Y.T., Li C., Fu L.-L., Zlotnicki V., Shum C.K., Yu Y, and V.Hjorleifsdottir, 2005. The 26 December 2004 tsunami source estimated from satellite radar altimetry and seismic waves, *Geophysical Research Letters* 32, L20601-5.

Tanioka Y., Yudhicara Y., Kususose T., Kathiroli S., Nishimura Y., Iwasaki S.-I., and K.Satake, 2006. Rupture process of the 2004 great Sumatra-Andaman earthquake estimated from tsunami waveforms, *Earth Planets Space*, 58, P.1–7.

Titov V., Rabinovich A.B., Mofield H.O., Thomson R.E., and F.I.Gonzalez, 2005. The global reach of the 26 December 2004 Sumatra tsunami, *Science* 309, 2045-2048.

Wilson M., 2005. Modeling the Sumatra-Andaman Earthquake reveals a complex, nonuniform rupture, *Phys.Today*, June, 19-21.

Kulikov E.A., Medvedev P.P., and S.S.Lappo, 2005. Registration from cosmos of tsunami 26 December 2004 in Indian Ocean, *Doklady RAS* 401, 537-542.

ISSN 8755-6839

SCIENCE OF **TSUNAMI HAZARDS**

Journal of Tsunami Society International

Volume 31 **Number 2** **2012**

GEODYNAMICS OF NAZCA RIDGE'S OBLIQUE SUBDUCTION AND MIGRATION - IMPLICATIONS FOR TSUNAMI GENERATION ALONG CENTRAL AND SOUTHERN PERU: Earthquake and Tsunami of 23 June 2001

George Pararas-Carayannis
Tsunami Society International, Honolulu, Hawaii, USA

ABSTRACT

Peru is in a region of considerable geologic and seismic complexity. Thrust faulting along the boundary where the Nazca plate subducts beneath the South American continent has created three distinct seismic zones. The angle of subduction of the Nazca oceanic plate beneath the South American plate is not uniform along the entire segment of the Peru-Chile Trench. Furthermore, subduction is affected by buoyancy forces of the bounding oceanic ridges and fractures - such as the Mendana Fracture Zone (MFZ) to the North and the Nazca Ridge to the South. This narrow zone is characterized by shallow earthquakes that can generate destructive tsunamis of varied intensities. The present study examines the significance of Nazca Ridge's oblique subduction and migration to the seismicity of Central/Southern Peru and to tsunami generation. The large tsunamigenic earthquake of 23 June 2001 is presented as a case study. This event generated a destructive, local tsunami that struck Peru's southern coasts with waves ranging from 3 to 4.6 meters (10-15 feet) and inland inundation that ranged from 1 to 3 km. In order to understand the near and far-field tsunamigenic efficiency of events along Central/Southern Peru and the significance of Nazca Ridge's oblique subduction, the present study examines further the geologic structure of the region and this quake's moment tensor analysis, energy release, fault rupture and the spatial distribution of aftershocks. Tsunami source mechanism characteristics for this event are presented, as inferred from seismic intensities, energy releases, fault plane solutions and the use of empirical relationships. The study concludes that the segment of subduction and faulting paralleling the Peru-Chile Trench from about 15^0 to 18^0 South, as well as the obliquity of convergent tectonic plate collision in this region, may be the reason for shorter rupture lengths of major earthquakes and the generation of only local destructive tsunamis.

Keywords: *Peru earthquake, tsunami, Peru-Chile Trench, seismotectonics, Nazca Ridge*

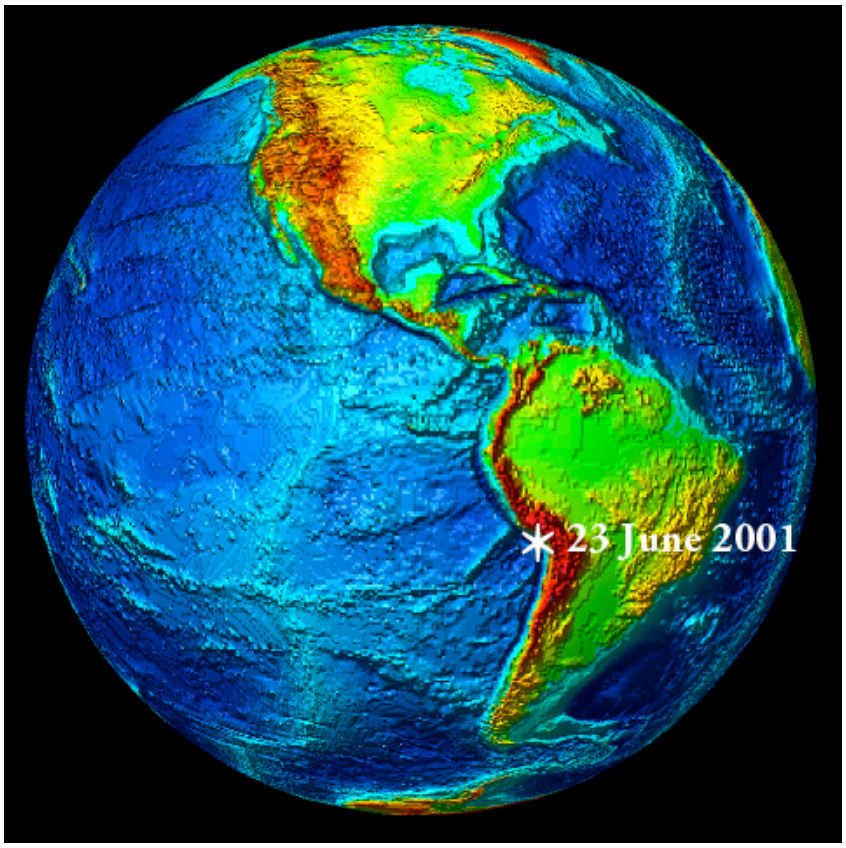

Figure 1. Epicenter of the 23 June 2001 Earthquake

1. INTRODUCTION

The present study examines Peru's geologic and seismic complexity and the possible impact oblique subducting fractures zones - such as the Mendana (MFZ) to the North and the Nazca Ridge to the South – can have on the tsunamigenic efficiency of large earthquakes. For reasons not well understood, this narrow zone in Peru is characterized by shallow large earthquakes that can generate destructive tsunamis of varied intensities. Specifically examined is the significance of Nazca Ridge's subduction and migration to the seismicity of Central/Southern Peru, using as a case study the great earthquake of 23 June 2001 and the destructive local tsunami that was generated. Although the near-field effects of this particular tsunami were severe, the far-field effects were insignificant. Only a small tsunami was observed or recorded at distant locations in the South and Central Pacific and in Japan. The following sections document the tectonic characteristics of this southern region of Peru, the earthquake's impact, the source mechanism of the tsunami, the near and far field effects, historical events in this region and an evaluation of the potential for future tsunamigenic earthquakes for this region.

2. THE EARTHQUAKE OF 23 JUNE 2001

The earthquake occurred at 2033 UTC (4:33 PM EDT, 3:33 PM local time) on Saturday, June 23, 2001. Various magnitude values were subsequently estimated, such as M_w=8.4 (Harvard CMT), M_w=8.3 (USGS), M_w=8.2 (Earthquake Information Center, Tokyo). Final assigned magnitude was M_w=8.4. The quake's epicenter was off the coast at 16.15S 73.40W (Fig. 2), just north of the coastal town of Ocoña in Southern Peru, approximately 375 miles (600 km) southeast of Lima and 120 miles (190 km) west of Arequipa.

Figure 2. The Earthquake and Tsunami affected the southern region of Peru from Arequipa to Tacna.

Focal Depth - The earthquake occurred along an area of high seismicity. Its focal depth was listed as shallow (less than 33 Km); however, because a large portion of the plate interface ruptured, it was difficult to estimate a single representative focal depth value, although the USGS Moment Tensor Solution gave a depth of only 9 km.

Major Aftershocks - The quake ruptured the Nazca-South American plate inter-phase and was subsequently followed by several large aftershocks, which were visible on the GPS times (Melbourne et al., 2002). Following the main quake, more than thirty significant aftershocks ($M_w > 4.0$) occurred through 7 July 2001 with the largest having a magnitude of 7.6 on July 7 (USGS 2001). Figure 3 shows the epicenter and the extent of aftershocks over that period following the main shock. Periodic aftershocks continued in subsequent days, weeks and months.

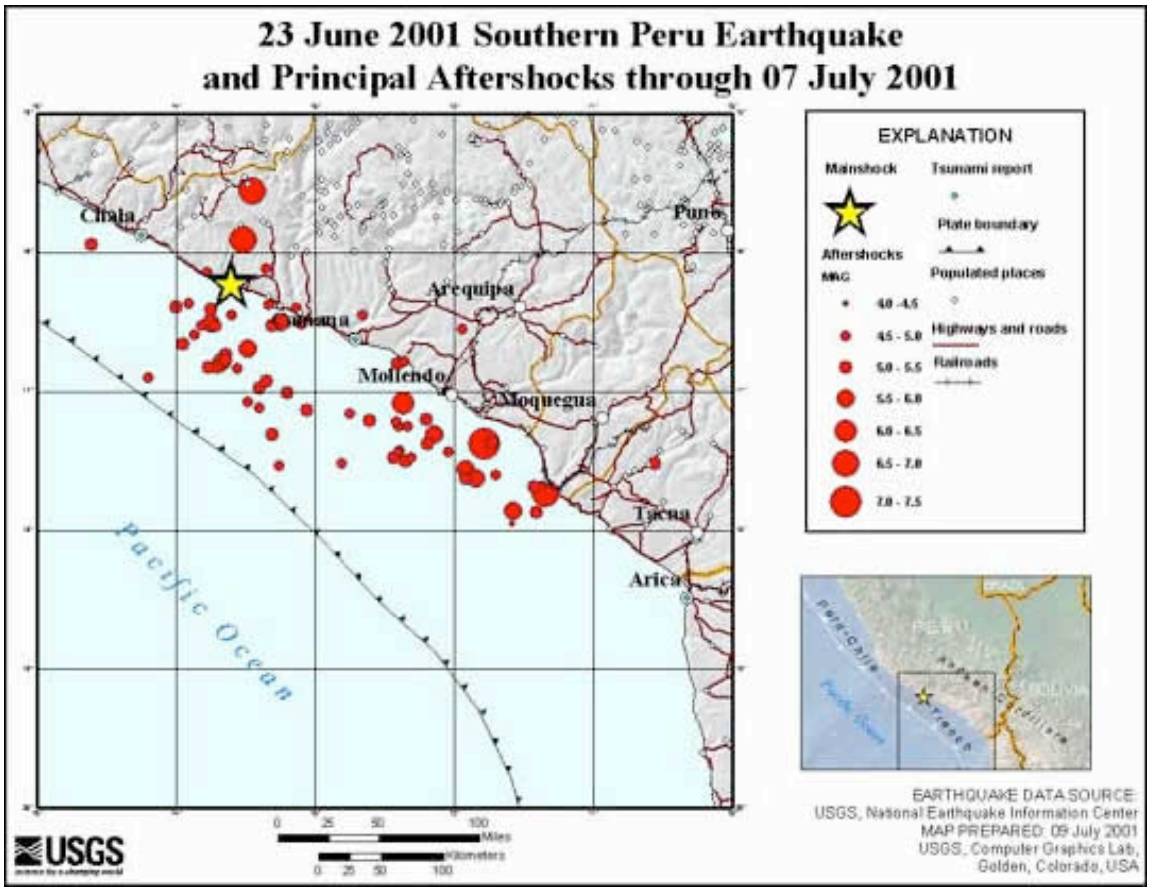

Figure 3. USGS Map of major Aftershocks through 7 July 2001

Focal Mechanism - The quake had a predominantly lateral strike slip with a smaller component of vertical dip slip motion. Figure 4 shows the determination of the earthquakes' focal mechanisms. Conventional magnitude estimates for this event ranged from M_s 8.2 to mantle magnitude M_m 8.6 (Okal and Talandier, 1989) – the latter corresponding to a seismic moment $M_0 = 4 \times 10^{28}$ dyn-cm. Other estimates of the seismic moment ranged from 1.2 to 4.9 $\times$ 10^{28} dyn-cm. The final Harvard determination, based on more data, gave the quake's strike at 310, the dip as 18, the slip as 63 and the energy release at 4.67 x 10^{28} dyn-cm.

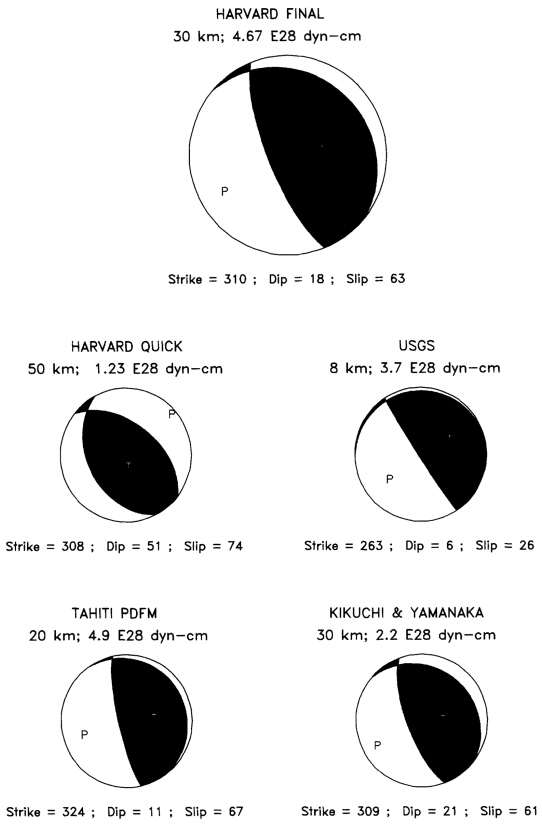

Figure 4. Focal Mechanisms as determined by Harvard, USGS, Tahiti PDFM and by Kikuchi & Yamanaka, 2001 (Univ. of Tokyo).

2.1 Earthquake Rupture

As stated, the 23 June 2001 earthquake ruptured a segment of the plate boundary between the Pacific and Nazca Plates. The rupture process may be linked to initial arc-parallel stresses caused by the bend in the South American subduction zone in this region and/or subduction of the Nazca Ridge (Macharé and Ortlieb, 1992). The initial rupture continued for about 70 km before encountering a 6,000 sq. km. area of the fault, which acted as temporary unbroken barrier for about 30 seconds. After this short interruption, the rupture front continued through this barrier at a low speed, slip and density of aftershocks, then for an estimated 200 km from the epicenter. The brief interruption of the rupture by the barrier was attributed to the regionally subducting fracture zone (Robinson et al. 2006). Similarly, based on broadband far-field seismograms with appropriate filters, parameterized and modeled the fault. The best fit solution of the model indicated that the rupture propagated in a southward direction at a very low speed of 1.6 km/sec with 80% of the final moment released as one patch 80 seconds after the onset of the rupture (Sladen et al., 2004). The significance of the subducting fracture zone, and the quake's slow rupture anomaly to tsunami generation is discussed in a subsequent section.

2.2 Earthquake Effects

The quake produced strong ground shaking that was felt in both southern Peru and northern Chile. Strong ground motions were also felt in many cities as far as Bolivia and Northern Chile. Even in Peru's capital, Lima (600 km away), homes collapsed, injuring several people.

According to reports, the ground motions in the affected region lasted for more than a minute. There was extensive destruction in southern Peru, particularly in the provinces of Arequipa, Moquegua and Tacna – where the highest intensities were observed (Fig. 5). In Arequipa and Moquegua, 80% of the homes were damaged as well as highways, water aqua-ducts and electrical systems. At the historic city of Arequipa (Fig. 6), Peru's second largest city with population of over one million people about 465 miles south of Lima, the quake destroyed historic homes and cathedrals, many of which had been rebuilt after the destructive 1868 earthquake. There were at least 73 reported fatalities in this area.

Figure 5. Region of Southern Peru mostly affected by the earthquake and tsunami of 23 June 2001.

In the southern city of Tacna, near the border with Chile, dozens of adobe homes were destroyed. Major damage occurred also in the zone known as La Yarada, where the electrical system was affected. There was extensive damage to the irrigation aqua-ducts in the valleys of Sama, Locumba and Tacna. Thirteen (13) people were reported killed in Tacna, and 8 in Ayacucho. Moquequa, a mining town about 1400 kms (865 miles) south of Lima, was also hard-hit. A landslide blocked one of the town's chief roads and many houses collapsed. Twenty-four people were reported killed and many more were injured. The Andean highland town of Characato was extensively damaged.

The quake practically wiped out the agricultural infrastructure of the region by causing the destruction of water reservoirs, canals and bridges. At Santa Rita de Sigua, the principal irrigation canal in this agricultural region, collapsed for about 300 meters - closing also the Pan-American Highway.

The number of dead, injured and missing continued to rise in the days following the main earthquake. According to Peru's Civil Defense Institute, as of June 26, 2001, 118 people had been killed, another 1,578 were injured, 53 were unaccounted and 47,696 were left homeless. A total of 21,189 homes were damaged or completely destroyed.

Figure 6. Extensive earthquake damage at Arequipa

2.2 Recent Earthquake Disasters in Peru

Destructive earthquakes occur with frequency throughout Peru. Prior to the 23 June 2001 event, the last major earthquake (7.7 magnitude) to strike along the Nazca subduction zone occurred on November 12, 1996. It killed 17 and injured about 1,500 people. On May 30, 1990, an earthquake (6.3 magnitude) in northern Peru killed 137 people. On May 31, 1970 another major earthquake (7.7 magnitude) killed approximately 70,000 people. On October 17, 1966, a strong earthquake (7.5 magnitude) off the coast of Pativilca severely damaged Central Peru. Also, this event generated a tsunami, which caused destruction along a 400 Km long coastal belt, from Chimbote in the North to San Juan in the South - including sectors of Lima-Callao (Pararas-Carayannis 1968, 1974). The USGS map below (Fig. 7) shows the epicenter of the 23 June 2001 earthquake, as well as the epicenters of major earthquakes to strike the region of Peru extending from 10^0 to 22^0 South Latitude.

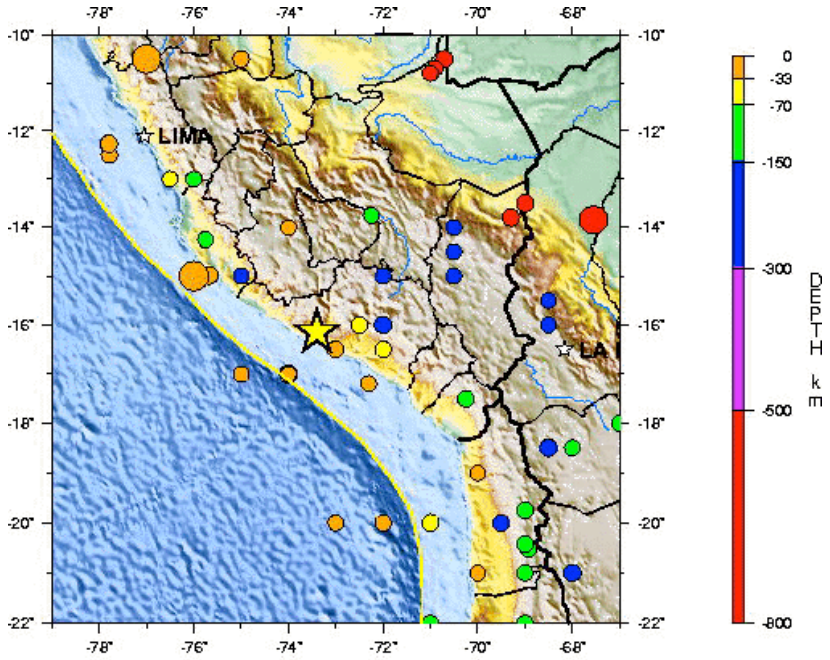

Figure 7. Epicenter of the 23 June 2001 Earthquake. Major Earthquakes since 1900 (USGS map)

3. THE TSUNAMI OF JUNE 23, 2001 IN SOUTHERN PERU

The June 23, 2001 earthquake generated a destructive, local tsunami, which struck the coastline, primarily near the epicenter region in southern Peru, approximately 20 minutes after the main shock. Based on the earthquake's large magnitude, initial visual reports and recordings from tide gauges in the region, the Pacific Tsunami Warning Center in Honolulu issued a Regional Tsunami Warning and Watch for Peru, Chile, Ecuador, Colombia, Panama, Nicaragua, El Salvador, Mexico and French Polynesia.

3.1 Near-Field Tsunami Impact

There were conflicting eyewitness reports as to the number of waves responsible for most of the damage in the area. It was reported that three to five separate waves struck and that either the second or third wave was the largest. Near-field damage was limited along the coastline from the town of Atico in the north, to Matarani in the south. Tsunami waves with run-ups ranging from 3 to 4.6 meters (10-15 feet) or more were reported. In some coastal areas, the tsunami waves swept one to two miles inland. Maximum tsunami run-up heights occurred along the coastlines of Chala-Camaná.

Camaná, a popular and picturesque summer resort of around 20,000 some 900 km (560 miles) south of Lima, was one of the hardest-hit areas by both the earthquake and the tsunami. The tsunami swept more than 800 meters (half-mile) inland over the town and its surrounding rice and sugarcane

fields. According to reports, 2,500 hectares of agricultural land were flooded. Maximum reported run-up exceeded 7 meters in some locations in the same area with greater than one-kilometer inland inundation. Eyewitness accounts from Camaná, described that four waves were responsible for most of the deaths and damage, the largest being the third. According to Peru's Civil Defense, at least 20 persons were reported drowned by the tsunami and another 60 persons as missing in this area.

La Punta, another popular resort area located along a narrow strip of beach immediately south of Camaná was also struck by powerful tsunami waves, which destroyed hundreds of homes, hotels and restaurants. Fortunately the tsunami struck when it was still wintertime in the southern hemisphere and beachfront communities were mostly deserted. The tsunami there was responsible for about 26 deaths with another 70 more reported missing in this area.

3.2 Far-Field Tsunami Effects

According to the Pacific Tsunami Warning Center's Bulletin in Honolulu, the following initial tsunami wave measurements (peak to trough) were reported from tide stations in Peru, Chile and the Galapagos (Table 1).

Table 1. Initial Tsunami Wave Recorded in Peru, Chile and the Galapagos

Tide Gauge Station	Measurement (Peak to through in m.	Wave Period (min.)
CALLAO (Peru)	0.4	14
SANTA CRUZ (Galapagos)	0.6	16
ARICA (Chile)	2.5	15
IQUIQUE (Chile)	1.5	20
ANTOFAGASTA (Chile)	0.9	18
CALDERA (Chile)	1.0	16
JUAN FERNANDEZ (Chile)	0.8	10
VALPARAISO (Chile)	0.5	18
SAN ANTONIO (Chile)	0.4	18
COQUIMBO (Chile)	1.0	18
CORRAL (Chile)	0.3	18
TALCAHUANO (Chile)	1.0	16
SAN ANTONIO (Chile)	0.3	15

The tsunami was observed or recorded by tide gauges across the Pacific Ocean. Small waves measuring a few centimeters were recorded or observed in the Southern and Central Pacific and as far away as Hawaii and Japan. The greatest tsunami oscillation of 30 cm peak to trough was recorded at Port Vila, Vanuatu, in the Southern Pacific. Additional tide gauges in the Central and South Pacific (Apia, Fanfuti, Kembla, Lautoka, Lombrum, Nukualofa, Rarotonga and Suva) recorded a small tsunami.

In Honolulu, Hawaii, a small influx of the tsunami was observed in the Kapalama and Nuuanu Streams, beginning at approximately 00:30 hours of June 24th. The observed water movements had an apparent period of 15-20 minutes.

3.3 Large Historical Tsunamis from Peru Earthquakes

Large tsunamigenic earthquakes occur frequently in Peru. The historic record shows that major earthquakes occurred on 9 July 1586, 13 November 1655, 20 October 1687, 28 October 1746, 30 March 1828, 24 May 1940 (M=8.4), 17 October 1966 (M= 7.5), 31 May 1970 (M= 7.7), 3O May 1990 (M=6.3) and 12 November 1996 (M=7.7). Of these, the earthquakes of 1586, 1687, 1746, 1828 and 1966 produced destructive tsunamis (Iida, Cox and Pararas-Carayannis, 1968; Pararas-Carayannis, 1968, 1974). To this list we must now add the June 23, 2001 event.

The 1868 Pacific-wide tsunami, characterized as the "Great Peru earthquake and tsunami", which destroyed Arica (then part of Peru), had its epicenter further south - in what is now northern Chile (around 18.5^0 South). The last major tsunami to strike Peru was on October 17, 1966. It affected a coastal belt 400 Km long, causing destruction from Chimbote in the North to San Juan in the South. The greatest wave at Callao had a range of 3.40 m height (range between maximum crest and trough) and tsunami waves exceeding 3 meters in amplitude (height above undisturbed water level) inundated La Punta, Chuito, Ancon, Huaura, Huacho, and the resort of Buenos Aires in the City of Trujillo. Devastating effects were experienced at the port of Casma (about 360 Km north of Lima) and at Calota Tortuga, where waves exceeded 6 meters in range. Tsunami destruction also occurred at Puerto Chimu and Culebras. The 1966 tsunami caused no damage outside Peru, but was recorded by tide gauges throughout the Pacific Ocean (Pararas-Carayannis, 1968, 1974).

3.4 Tsunami Generating Area

The azimuthal orientation of a tsunamigenic area can be estimated from seismic and oceanographic data, as well as from the distribution of major aftershocks immediately following the main quake (Pararas-Carayannis, 1965, 1968, 1972, 1974). The nature of the first seismic motion related to an earthquake depends on the crustal displacement at the source. The impulse of P (compression) waves indicates a vibration in a plane containing the great circle that passes through the epicenter and the seismic station recording the earthquake (Galitzin, 1909). If the first impulse on the vertical component of the seismograph is up, the first phase of P wave is a compression, so the composition of north south and east west is in a direction away from the epicenter. A composition of the three components gives the direction of the first displacement of the ground, which however is not the exact direction of the path of the incident wave. It is rather the combination of the amplitudes of the incident P wave and the reflected P and S (shear) waves that give an indication of the motion of the surface of the ground at the source. These are significant parameters in understanding the tsunami source mechanism. This understanding has greatly improved with the use of data from broadband seismometers.

Although these are basic concepts, it may be helpful to summarize them. In brief, a single force

sends compression waves into a half space and rarefaction waves into the other half space; a couple sends alternate compressions and rarefactions into quarter spaces (Nakano, 1923). Modal planes of the focus can be deduced from recordings of compressions and rarefactions (Byerly, 1955). Such a pattern can be considered a function of the azimuth to be expected from a seismic source. From this and the distribution of aftershocks, the tsunamigenic area can be approximated.

Additionally, the tsunamigenic area of an earthquake can be deduced indirectly from oceanographic parameters by refracting tsunami waves back to the source from tide gauge stations, which recorded the tsunami, and for a length of time equal to the travel time to each station. Using several stations and based on water wave refraction analysis, an approximate envelop can be established giving the approximate orientation and dimensions of the tsunamigenic area (Pararas-Carayannis, 1965, 1972, 1974).

Review of aftershock distribution following the June 23, 2001 earthquake main shock and analysis of the moment tensor, indicated initially that the fault rupture and the tsunamigenic area (an approximate ellipse), had a general trend striking at 284 degrees with a dip=7 and a slip 45. However, and as indicated previously, the final Harvard determination gave the quake's strike at 310^0, the dip as 18, and the slip as 63. The distribution of aftershocks at sea had a similar azimuthally NW-SE distribution paralleling the Peru coastline, thus defining the tsunami generating area as approximated in Fig. 8.

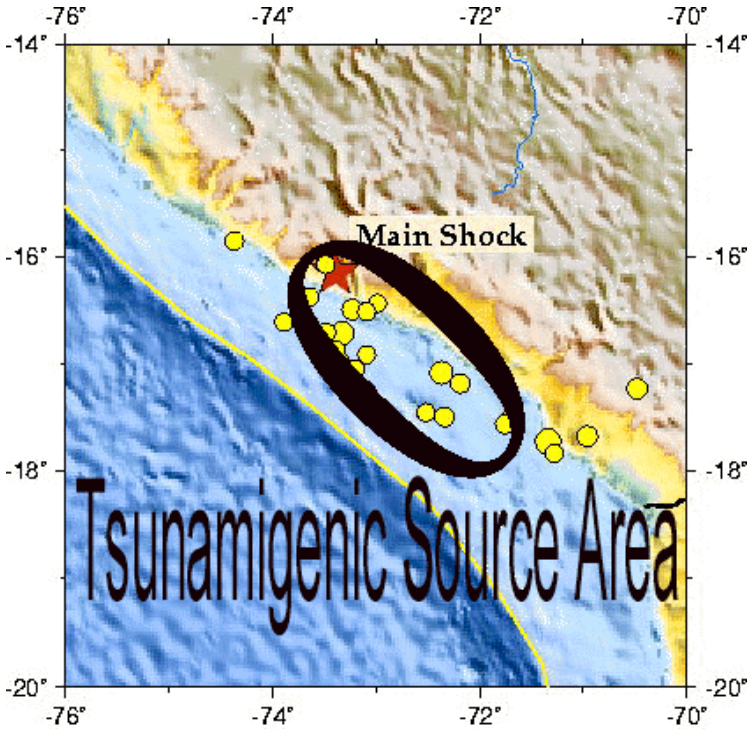

Fig. 8 The Generating Area of the 23 June 2001 tsunami.

The azimuthal orientation of the tsunami generating area shown in this map is in agreement with the general trend of the fault systems, the Andean Mountains, and the Peru-Chile Trench in this region.

The dimensions of the tsunami generating area given in the literature varied depending on the use of the seismic inversion of the rupture process that was used. For example, by using a shallow-dipping nodal plane consistent with an inter-plate thrust earthquake along the Peru subduction zone and assuming a magnitude of only Mw=8.2, the moment distribution showed a rupture area that was 210 km long and 120 km wide (Kikuchi and Yamanaka, 2001). However, according to other studies discussed earlier (Macharé and Ortlieb, 1992), the initial rupture of the 2001 earthquake was 70 km before encountering a 6,000 sq. km. area of the fault, which acted as a temporary unbroken barrier for about 30 seconds. As indicated, after this short interruption and possible stress transference, the rupture front of perhaps a different event continued in a southeasterly direction through this barrier on another segment for another 200 km. Therefore, the combined tsunami generating areas of perhaps two distinct events - separated in time by 30 seconds - must have been at least 300 km long and perhaps wider than 210 km. These dimensions of the tsunami generating area are also supported by the aftershock distribution and the rupture, which extended southeast from the epicenter to the vicinity of Ilo, about 150 km north of the Chilean border. Based on the estimated fault length, the tsunami generating area is roughly calculated to cover about 17,200 sq. km.

3.5 Ocean Floor Displacements and Initial Tsunami Height

Dynamic motions during the earthquake and co-seismic vertical displacements provided the initial conditions for tsunami generation and propagation. However, since the earthquake's rupture area extended landward of the coastline, only a part of the co-seismic deformation contributed to tsunami generation. These crustal displacements were of a dipole nature (negative and positive) along a thrust fault approximately paralleling the Peruvian coast. The co-seismic vertical displacements probably varied along the different segments along the rift. The maximum vertical uplifted movement is estimated to have been about 1.8 m on the continental side of the rift and about 1.8 downward on the oceanic side of the rift. However, these represent maximum crustal displacement values diminishing away from the rift zone. Upward, ground displacements also occurred on land along the affected coastal area, as well as other significant co-seismic lateral movements, which may have disturbed sedimentary layers of the accretionary prism, thus contributing also to the tsunami height.

Since the June 23, 2001 earthquake in Peru was very shallow in depth (9 km), this may have limited the extent of the displacements and thus the tsunamigenic area. The quake had a predominantly lateral strike slip with a smaller component of vertical dip slip motion. It is the latter motion that contributes significantly to tsunami generation. Based on empirical relationships we can estimate the total displacement which is the resultant of the horizontal strike slip, "X", and the vertical dip-slip, Z, related by:

Total Displacement = $X^2 + z^2$ (raised to ½)

The horizontal strike slip and the vertical dip slip for this event are not known with certainty - although the maximum vertical crustal displacement is estimated at 1.8 meters. However, statistical relationships between maximum crustal displacement and earthquake magnitude M were

compiled in the past and working curves have been plotted (Wilson 1964, 1969). Although such empirically derived curves display scatter of data - possibly because of differences in the focal depth and geology of each region associated with each seismic event - a median value can be selected as being reasonable for shallow-focus tsunamigenic earthquakes. For the June 23, 2001 earthquake (Mw = 8.4), the median value of crustal displacement along the fault taken from such curve is 5.4m. These were the estimated co-seismic displacements and offsets. However, GPS data collected subsequently over a two-year period, indicated additional post-seismic offsets and deformation, which were slowly decreasing. The observed co-seismic subsidence was followed by post-seismic vertical uplift and slow aseismic westward movement of the Peruvian coastline (Melbourne et al, 2002, Perfettini et al, 2005). Of course such post-seismic deformation does not contribute to tsunami generation.

If we assume an extreme ratio of strike-slip: Dip-slip, 10:3, then dip-slip, or vertical movement of the ocean floor along the fault, is estimated from the equation above to be, Z = 1.78m. Preliminary source inversions for the main shock indicated thrust slip ranging from 1 to 8 meters over a broad asperity that was 200 km by 300 km centered to the southwest of Arequipa (Kikuchi and Yamanaga, 2001). However, this occurred mainly over a land area and not in the ocean.

Long ago it was established that vertical displacements of a seismotectonic block responsible for tsunami generation will decay exponentially with distance normal to the fault in accordance to the elastic rebound theory (Reid 1910). Thus, the ocean area affected by such displacements - the tsunami generating area - is an approximate ellipse in which the fault occupies the major axis, which possibly coincides with the rupture zone if it is located in the ocean. The leading tsunami waves are generated from the periphery of this area - and their arrival at nearby stations – is also indicative of the initial ocean floor displacement. Maximum run-up on the shore, is generally caused by the crest of the tsunami wave near the fault.

Based on the above assumptions of vertical ocean floor displacements, the initial tsunami height in the generating area is estimated at a maximum of 1.5 - 1.78 meters above the undisturbed sea level. Given, therefore, the magnitude, depth and epicenter of the earthquake and utilizing the assumptions and empirical relationships outlined here, the run-up along Southern Peru from tsunamis originating from this seismic region can be roughly approximated. Considering that the measured waves reaching the immediate coastline of Southern Peru had maximum run-ups of about 5 meters, the shoaling and resonance amplification factor on this coast for local tsunamis is estimated to be about 2.8 times the maximum deep water value (1.78 x 2.8 = 4.99 meters).

As stated, the earthquake's focal mechanism indicates that the tsunami was generated from dipole type of crustal movements, which involved vertical displacements. However, the earthquake also involved lateral movements, which must have affected the sediment layers in the accretionary prism on the landward side of the fault. Such lateral compression of sediment layers probably resulted in up-thrusts in this zone, which contributed to the formation and destructiveness of the tsunami locally.

3.6 Fault Length

Statistical relationships between fault length L (Km) and earthquake magnitude (M) have been also worked out in the past. Using such a statistical relationship as documented in the literature

(Ambraseys and Zatopek, 1968), we can estimate the fault length to be:

$$\text{Log } L = 1.13\ M - 6.4$$

If we assume that the earthquake of June 23, 2001 had the equivalent Richter magnitude of 8.1, the fault length estimated by such early empirical relationships would be only about 152 km. However since such empirical relationships relate to Richter magnitude and not to Moment Magnitude (estimated at Mw=8.4) they do not provide a reliable estimate. As stated, seismic inversion of the rupture process indicated that the actual fault length for this event was much longer. The fault was at least 300 km long. The width of the affected area was as much as 210 km or more.

4.5 Tsunami Energy

The 2001 Peru earthquake (Mw =8.4) released the largest moment of any event in the previous 30 years and produced over 50 cm of co-seismic offset at the GPS tracking station at Arequipa (AREQ), which is located about 100 km from the coast (Melbourne et al., 2002). Based on the estimated fault length, the tsunami generating area is roughly calculated to cover about 17,200 sq. km. According to the final Harvard tensor analysis, the energy release of the earthquake was 4.67×10^{28} dyn-cm. The energy that went into tsunami generation can be estimated on the basis of the source dimensions and the energy that resulted in the uplift or depression of the ocean floor. Assuming that the total energy is equal to the potential energy of the uplifted or depressed volume of water, the total energy for the tsunami can be roughly approximated by:

$$(E_t) = 1/6\ p.g.h^2$$

Where E_t = Total energy

p = 1.03 g/cm = Density of sea water

g = 980 cm/sec = gravitational acceleration

h = Assumed average height of crustal displacement (throughout the tsunamigenic area) = .55 m

Since the Tsunami generating area (A) is 17,200 Km, the energy of the tsunami can be estimated to be

$$E = 1/6\ p.g.h^2.A = 1/6(1.03)(.980)(10^3)(10^4)(.55^2)(17{,}200 \text{ sq. km}) = 8.99 \times 10^{19} \text{ ergs (or dyn-cm).}$$

where 1 erg = g cm sec.

Considering that the energy of the June 23, 2001 earthquake (M_w 8.4) was very large, the energy

responsible for tsunami generation was a small fraction of the total earthquake energy, which – according to the Harvard final estimate was as much as 4.67 x 10^{28} dyn-cm.

5. DISCUSSION

As illustrated by Fig. 9, Central and Southern Peru is a region of high seismicity caused by active interactions of major tectonic plates as well as oblique subduction of migrating oceanic ridges, which influence the size and depth of coastal earthquakes and the generation of tsunamis. The following sections review the significance of such interactive processes to tsunami generation. Although the discussion pertains to Central/Southern Peru using primarily the 23 June 2001 tsunami as a case study, the analysis is also applicable to other areas where oceanic ridges subduct obliquely under continents, as for example along the North America continent, along Chile and elsewhere.

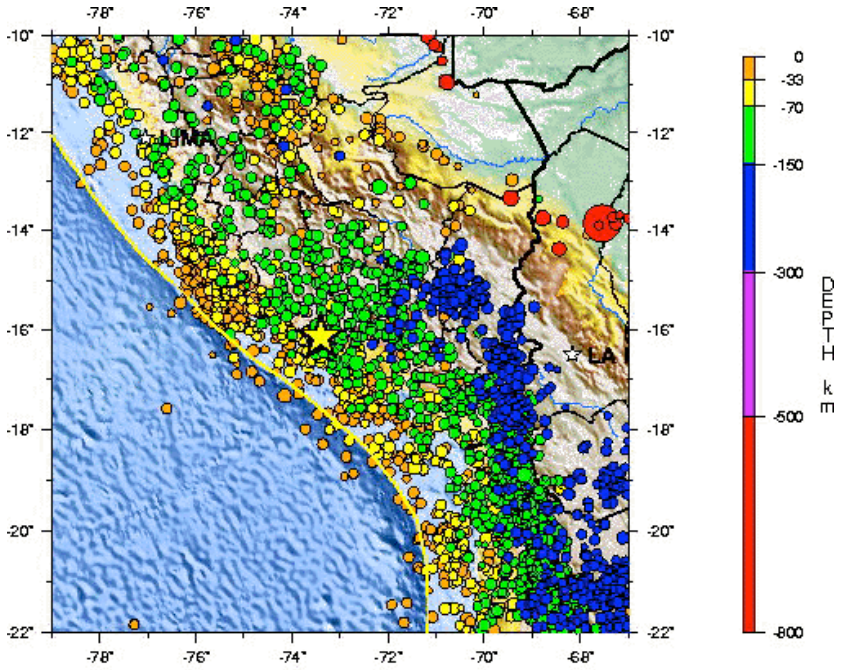

Fig. 9 Epicenter of the June 23, 2001 Earthquake / Seismicity of Southern Peru (USGS graphic)

5.1 Significance of Nazca Ridge's Oblique Subduction and Migration to the Seismicity of Central/Southern Peru and to Tsunami Generation

Southern Peru is a region of considerable geologic and seismic complexity because of the obliquity of converging tectonic plates at about 77 mm per year. However, the angle of subduction of the Nazca oceanic plate beneath the South American plate is not uniform along the entire segment of the Peru-Chile Trench fronting Peru. Furthermore the angle of subduction is apparently affected by buoyancy

forces of the bounding oceanic ridges and fractures - such as the Mendana Fracture Zone (MFZ) to the North and the Nazca Ridge to the South in Northern/Central Peru, as previously documented (Pararas-Carayannis, 2007; Sacks, 1983).

The overall subduction in the Peru segment of the Trench begins with a dip of about 30 degrees. However, seismic reflections studies indicate that it then flattens out and becomes sub-horizontal between 100 and 150 km depth beneath Peru, before steepening and descending into the earth's mantle. Also, seismic studies indicate that the flat slab segment exhibits a 20-40 km lithospheric "sag", approximately mid way between relative highs from 5^0 to 13^0 South. This suggests a double buoyant plateau model, with the Nazca Plate supported by two light bodies - the Mendana Fracture Zone (MFZ) to the North and the Nazca Ridge to the South. Such "saging" due to buoyancy forces would be expected to affect the source mechanisms of earthquakes, particularly near areas where an oceanic ridge, such as the Nazca Ridge, intercepts the continent. In fact the epicenter of the earthquake of August 15, 2007 was near this "sag" at 13.353^0 S, very close to the region of Nazca Ridge convergence with the South American continent. However, the 23 June 2001 earthquake was at 16.15^0S, 73.40^0W, south of Nazca Ridge's subduction zone, near a geologically anomalous, syntaxial region of Peru where there is a higher density of shallow earthquakes and a change in the obliquity of tectonic subduction (Fig. 10).

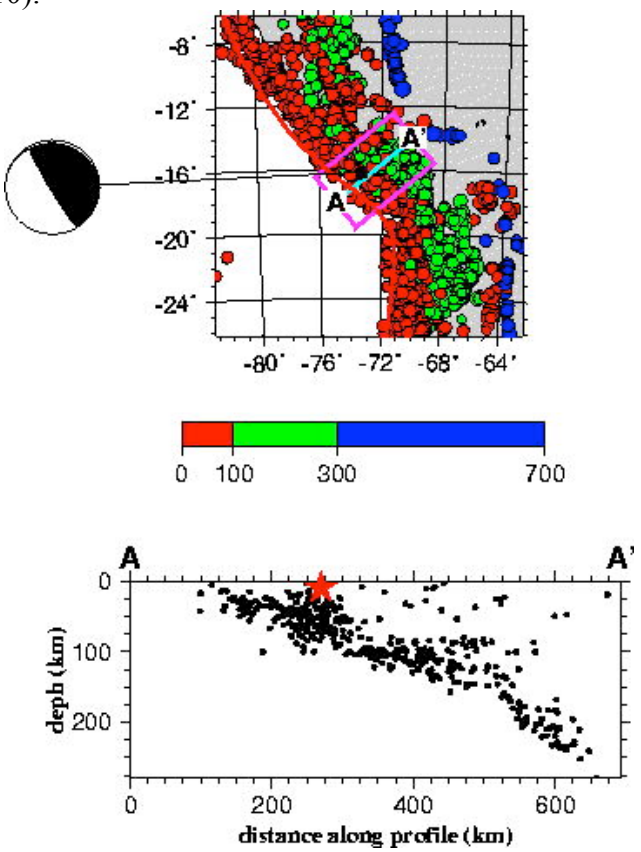

Figure 10. Focal mechanism of the 23 June 2001 Earthquake. Distribution of the foci of intermediate and deeper earthquakes underneath the continent in the South Peru region (Internet graphic)

5.2 Examination of Seismic Anomalies and Possible Effects on Tsunami Generation

Let us examine further the Nazca Ridge and what causes the observed seismic anomalies near the region where the 23 June 2001 tsunami was generated. The Ridge originated at the Easter Island hotspot. Review the Ridge's subduction process beneath the South American continent indicates that it is oblique and occurs from about 13.5^0 to 15.6^0 South and has been responsible for varying uplift rates and extensive crustal deformation of the upper plate from the northeast to southwest along the Peruvian coast during the Quaternary and thereafter (Pararas-Carayannis, 2007). The Ridge's varying rates of convergence and oblique northeastward orientation relative to the east-west direction of plate convergence has resulted in an approximate 70 mm/yr southeastward migration of the zone of the Ridge's subduction beneath the Peruvian coast. This is evident by a narrowing of the shelf, a westward shift of the coastline and the presence of marine terraces.

Above the southern flank of the Nazca Ridge, the coast is still rising at a fast rate as determined from studies of marine terraces on the coasts of Peru and Chile (Hsu, 1992; Hampel, 2002). The pattern of faster uplift above the southern flank and the slower uplift above the northern flank of the Ridge is a predictable consequence of the Ridge's oblique subduction. However, this has created anomalies which affect also the seismicity of the region on both sides of the Nazca Ridge's subduction zone and has created asperities which limit the length of earthquake ruptures, the depth of quakes, as well the tsunami generating sources and processes. The 23 June 2001 earthquake's epicenter at 16.15^0 was just south of the Ridge's southern flank and north of the generating area where the great 1868 Arica tsunami was generated. Thus, the 2001 event did not have as great of a rupture zone as that of 1868.

In addition to seismic reflection studies, review of studies of mineral concentrations provides additional clues for geotectonic anomalies that can also help determine whether a destructive tsunami may be generated along a specific segment of the active marginal convergence zone in Southern Peru. Magmatic-hydrothermal ore deposit concentrations were found in regions of Peru associated with aseismic ridge subduction (Fig. 11).

Specifically, magmatic-hydrothermal ore deposits found in the Andes and along certain coastal regions of Peru have been correlated to past distinct and sudden metallogenetic episodes during the last 200 Ma - episodes not necessarily associated with the progressive eastward movement of the Nazca plate beneath the continental South American plate (Rosenbaum et al. 2005 A, B).

The localized concentrations of ore deposits suggest the existence of crustal heterogeneities within the subducting oceanic plate (the Nazca plate) - which are particularly prevalent in the Southern Central Peru region. These heterogeneities may be caused by the suspected crustal buoyancy anomalies, which affect the dynamics of the subduction system in this particular region of Peru (near the Nazca Ridge in central Peru where the August 15, 2007 earthquake occurred). Accordingly, there may be laterally migrating zones of flat ridge subduction which could account why the great M_W+8.1 magnitude earthquake of 15 August 2007 did not generate a tsunami of great far-field significance as other earthquakes further north or further south have done (Pararas-Carayannis, 2007).

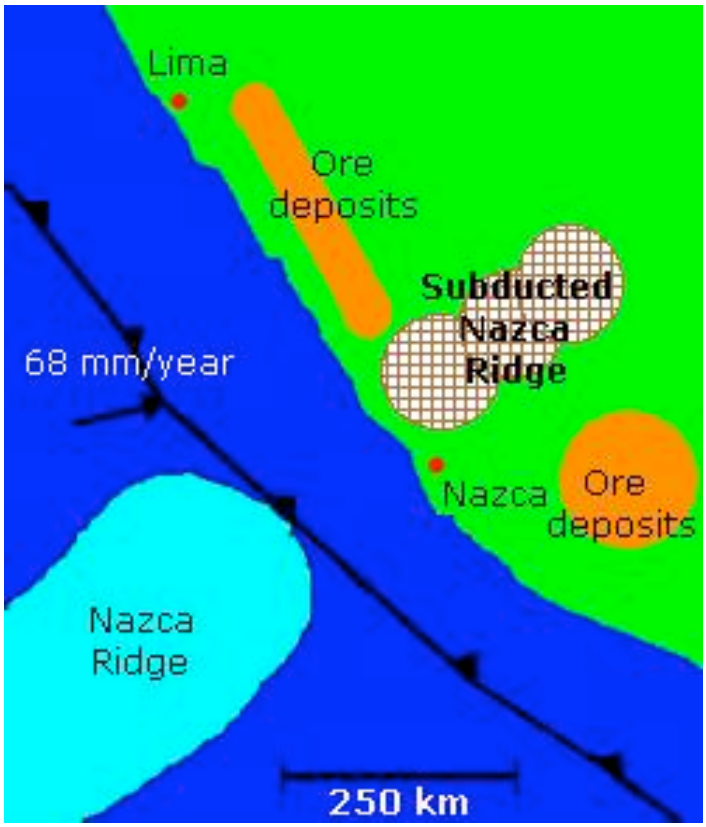

Fig. 11. Localized concentrations of ore deposits suggesting the existence of crustal heterogeneities within the subducting oceanic plate (After Rosenbaum et al. 2005 A, B)

5.3 Examination of the Earthquake Rupture Effects on Tsunami Generation

Let us further examine the tectonic geometries of Central and Southern Peru and the implications of Nazca Ridge's subduction to seismic anomalies that can affect tsunami generation. Specifically, in the vicinity of the Nazca Ridge intersection with the South American continent, it appears that there is a northward kink in the subducting extension - which would also support the existence of different tectonic geometry by northward-trending lateral compressive forces - the same forces that have formed the Paracas peninsula ending at Punta Huacos. Thus, the length of earthquake-caused ruptures in this region is limited. This is a reasonable explanation why the earthquake of 15 August 2007 in the region did not generate a destructive tsunami elsewhere except in the immediate region (Pararas-Carayannis, 2007). As stated, apparent changes in the geometry of subduction of the Nazca Ridge as well as heterogeneous compressive forces affect tsunami generating mechanisms along Central and Southern Peru by limiting the extent of earthquake ruptures and areas of crustal displacements. This holds true for many other areas where similar oceanic ridges intersect continents. Figure 12 illustrates the evolution of tectonic anomalies by the compressive forces generated by the subduction of Nazca Ridge and migration.

From this preliminary analysis we can reasonably conclude that earthquakes further north and south of the Nazca Ridge have the potential of generating local destructive tsunamis in Peru with more extensive far-field impact. However earthquakes that occur in the region near the Nazca Ridge intersection appear to have shorter ruptures and a diminished potential for far-field destructive tsunamis.

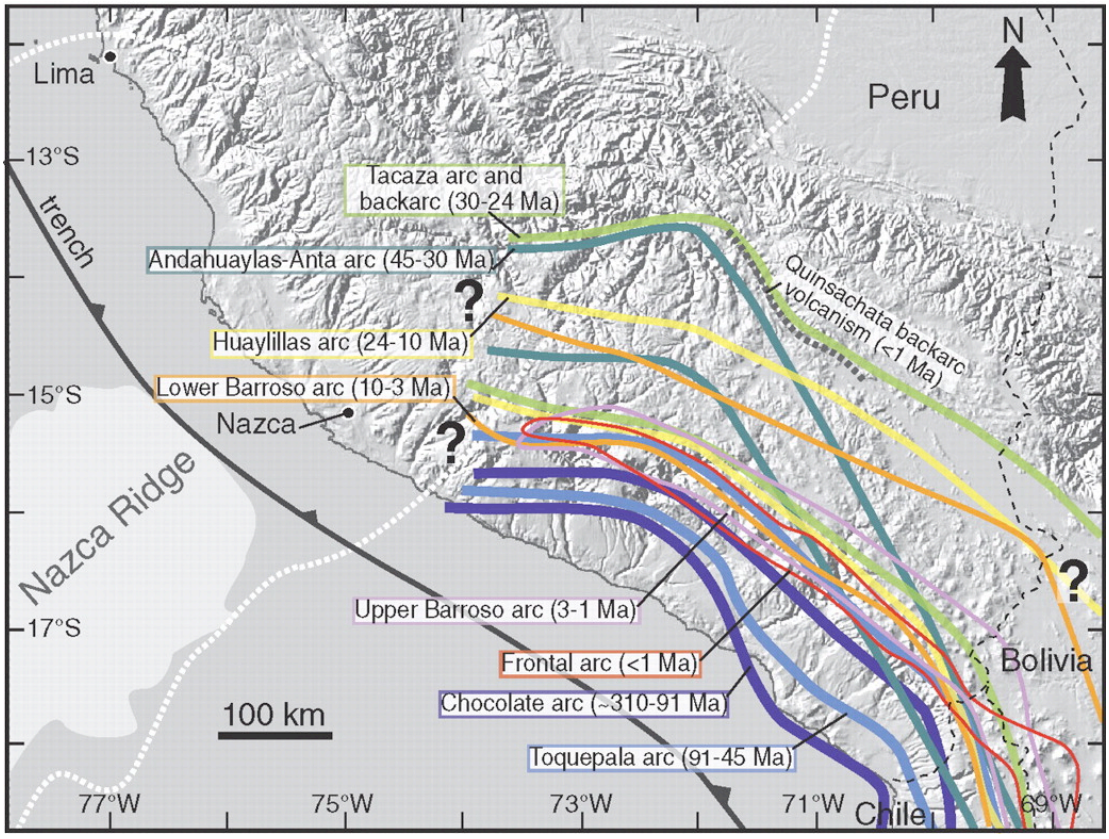

Figure 12. Evolution of tectonic anomalies in Southern Peru generated by compressive forces of Nazca Ridge's subduction and migration (Internet graphic).

Further review of earthquake rupture processes for this southern region of Peru indicates that they are apparently linked to initial arc-parallel stresses caused by the bend in the South American subduction zone and/or the subduction of the Nazca Ridge and on other anomalous structures. These structures appear to also limit the length of ruptures and of their speeds, thus limiting also the size of a tsunami's generation area and its source parameters. This limitation is particularly significant in that tsunamis that are generated in the segment ranging from about 16^0 to 18^0 South Latitude, can be destructive locally but do not seem pose a threat for the rest of the Pacific. This is also supported by the historical records of tsunamis described earlier (Pararas-Carayannis, 2007).

5.4 Examination of Spatiotemporal Anomalies of the 23 June 2001 Earthquake and Effect on Tsunami Generation

There is a noticeable higher density of shallow earthquakes near the subduction zone of the Nazca Ridge (Fig. 12). Apparently, events in this central/southern region of Peru are controlled by local tectonic anomalies. For example, the great earthquake of 23 June 2001 in the region was anomalous since it involved spatiotemporal slip distributions that differed significantly from the predominantly unilateral or bilateral rupture expansion that is typical for other great earthquakes elsewhere (Lay et al, 2010). As documented in the literature (Macharé and Ortlieb, 1992), the initial rupture of the 2001 earthquake continued for about 70 km before encountering a 6,000 sq. km. area of the fault which acted as a temporary unbroken barrier for about 30 seconds. After this short temporal interruption, the rupture front continued in a southeasterly direction through this barrier, but at the rather low speed of 1.6 km/sec, for about 200 km. Finally, 80% of the final moment was released as one patch 80 seconds after the onset of the rupture (Sladen et al., 2004). As indicated, the brief interruption of the rupture by the barrier was attributed to the regionally subducting Nazca Ridge - fracture zone (Robinson et al. 2006). The slow rupture speed after the barrier, indicates the existence of sedimentary layers within an accretionary prism which, when up-thrusted by vertical as well as lateral crustal displacements, contributed significantly to a more efficient local tsunami generation.

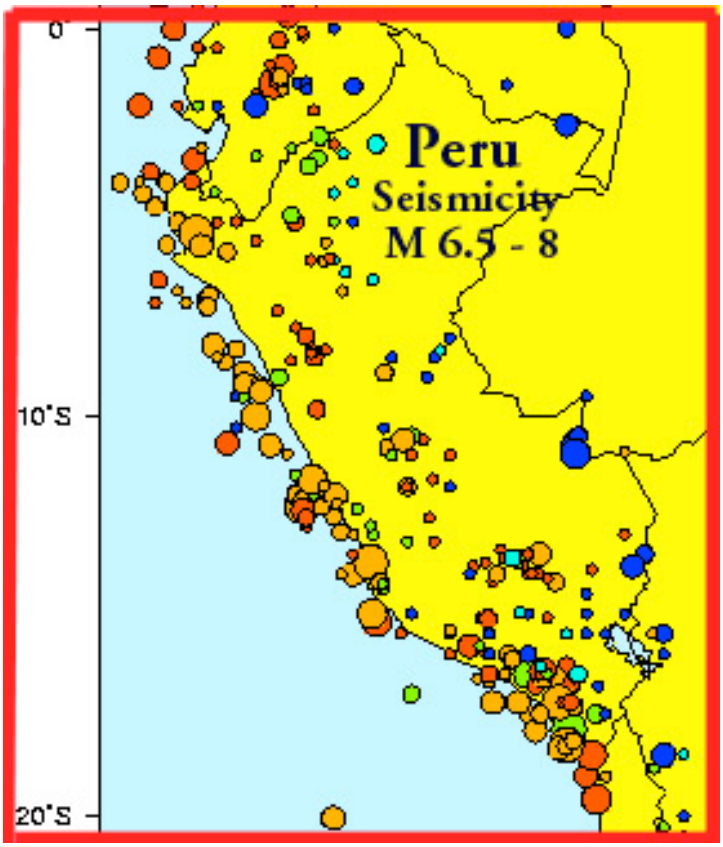

Figure 12. Seismicity of Peru (Magnitude 6.5 - 8) (Pararas-Carayannis, 2007)

5.5 Tsunamigenic Potential along Southern Peru

As documented, the Peru-Chile Trench is a manifestation of very active subduction along the South American continent. Most of the destructive tsunamis along the South American coast have been generated from major, shallow earthquakes, east but in close proximity to the Peru-Chile Trench. Deeper earthquakes along the Beniof Zone (which is quite wide and flat in this area of Southern Peru) do not produce tsunamis). Historically, the large earthquakes along the Peru-Chile Trench above latitude 16^0 South have produced locally destructive tsunamis but not destructive Pacific-wide tsunamis. For example, the 1966 tsunami which was generated by a large earthquake in the central part of Peru's seismic zone 4, had a rather short rupture of about 120 km (Pararas-Carayannis, 1968, 1974). It did not produce a Pacific-wide tsunami. Similarly, the June 23, 2001 Peru earthquake had a relatively short rupture (estimated at max. 300 km) and did not generate a large Pacific- wide tsunami.

The gradients in obliquity appear to change south of 18.5^0 as a consequence of the geometry of tectonic plate motions. In this region, the rupture lengths of major earthquakes are longer and the tsunamigenic potential is greater. The real destructive Pacific-wide tsunamis have been generated along the coast of Chile. The 1868 Pacific wide tsunami, characterized as the "Great Peru earthquake and tsunami", which destroyed Arica (then part of Peru), had its epicenter further south - in what is now northern Chile (around 18.5^0 South).

The May 9, 1877 (Mw 8.8) quake near Iquique, had a rupture of about 420 km along the coast of Chile and extended from 18^0 to 23^0 South latitude and generated a destructive Pacific-wide tsunami. The wave heights of that event reached 24 meters in Chile and up to 5 meters in Hawaii (Pararas-Carayannis 1969; Pararas-Carayannis and Calebaugh, 1977).

The November 10, 1922 earthquake (M_t 8.7) in Northern Chile, had a rupture of about 300-450 km-long, extending from about 26.1^0 to 29.6^0 South. It generated also a Pacific-wide tsunami - although not as large as that generated by the 1877 or 1868 earthquakes. Finally, the 1960 Pacific-wide tsunami was generated by another great earthquake which had its epicenter at about 37.5^0 South. The reason this tsunami was so destructive in Hawaii, Japan and elsewhere in the Pacific, was that the 1960 earthquake's rupture extended along a strike length of about 900 -1000 km.

More recently, the great (M_w=8.8) earthquake of 27 February 2010 occurred along a segment of Chile's central seismic zone - extending from about 33ºS to 37ºS latitude, just south of the Juan Fernández ridge. Because of the proximity to the ridge, this earthquake also had a complicated rupture process and co-seismic displacements (Fig. 13). The total rupture was about 550 km long and extended to about 50 km in depth. This is also an area where active, oblique subduction of the Nazca tectonic plate below South America occurs at the high rate of up to 80 mm per year. The unusual rupturing process of the 2010 earthquake also released energy gradually, which could partially account for the less severe near and far-field tsunami effects. Apparently the geodynamics of the Juan Fernández ridge had an impact on this earthquake's rupture, crustal displacements and the generation of the tsunami (Pararas-Carayannis, 2010).

In conclusion, it appears that the obliquity of convergent tectonic plate boundaries and the subduction of oceanic ridges along southern Peru may be the reason for the shorter rupture lengths of earthquakes and the generation of only local destructive tsunamis. The historic record also supports such conclusion.

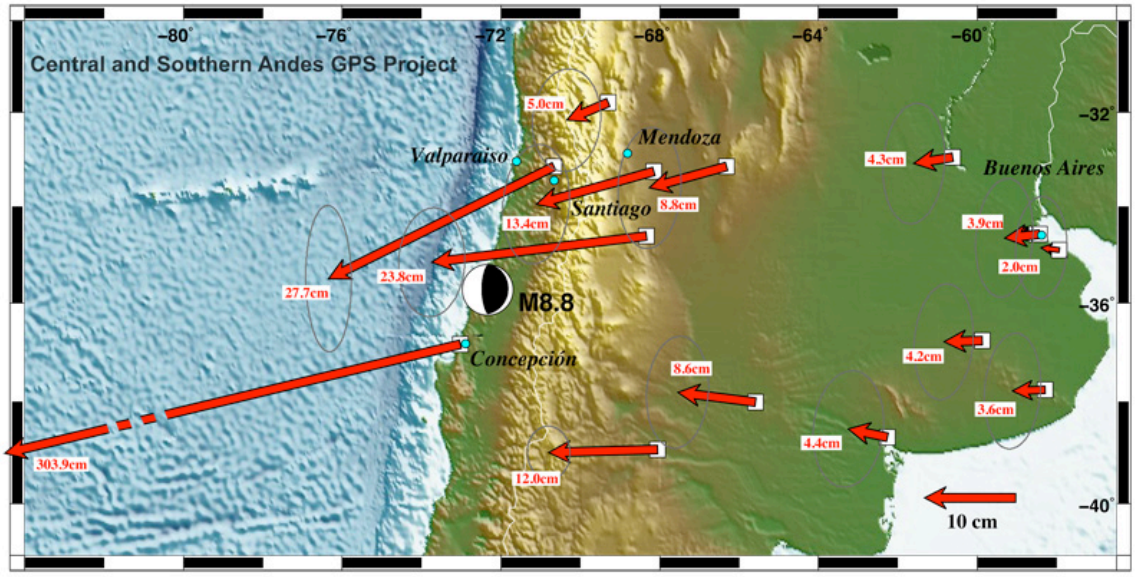

Fig. 13. Co-seismic displacement field associated with the February 27, 2010 Maule earthquake in south-central Chile, based on GPS Geodetic measurements (James Foster and Ben Brooks, University of Hawaii). Note proximity of the epicenter to the Juan Fernández ridge

5. SUMMARY AND CONCLUSIONS

The angle of subduction of the Nazca oceanic plate beneath the South American plate is not uniform along the entire length of the Peru-Chile Trench and particularly along the segment fronting Peru. Subduction along Peru is affected by buoyancy forces of the bounding oceanic ridges and fractures - such as the Mendana Fracture Zone (MFZ) to the North and the Nazca Ridge to the South – which create "saging" and anomalies which affect the source mechanisms of earthquakes.

The geodynamics of Nazca ridge in the vicinity of Central and Southern Peru involve oblique subduction and migration which is changing the geologic structure of the region. The Ridge's oblique subduction process beneath the South American continent occurs from about 13.5^0 to 15.6^0 South and has been responsible for varying uplift rates and extensive crustal deformation of the upper plate from the northeast to southwest along the Peruvian coast. The crustal buoyancy anomalies on both sides of the Nazca Ridge's subduction zone have affected also the seismicity of the region and have created asperities which limit the length of earthquake ruptures, as well as the tsunami generating sources and processes. Earthquakes near the Nazca Ridge intersection appear to have shorter ruptures and a diminished potential for far-field destructive tsunamis. This limitation is particularly significant for tsunamis generated along the segment ranging from about 16^0 to 18^0 South. The large tsunamigenic earthquakes of August 15, 2007 north of the Nazca Ridge and of 23 June 2001 to the south, are typical events that can be expected along the coasts of Central and South Peru. The local destructive tsunamis that were generated did not have any significant far-field impacts.

The gradients in obliquity appear to change south of 18.5^0 South as a consequence of the geometry of tectonic plate motions. In this region, the rupture lengths of major earthquakes are longer and the tsunamigenic potential for Pacific-wide impact, greater.

REFERENCES

Byerly, P., 1955. "Nature of Faulting as Deduced from Seismograms", Geol. Soc. Am. Spec. Paper 62, 75-86.

Fisher, R. L. and Raitt, W. R., 1962. "Topography and Structure of the Peru-Chile Trench", Deep Sea Res., 9, 423-443.

Galitzin, B.,1909. "Zur Frage der Bestimmung des Azimuts der Epizentrums eines Bebens"; Assoc. Internat. de Sismologie, C. R. Zermatt, 1909, pp. 132-141.

Gutenberg, B. and Richter, C. F., 1954. "Seismicity of the Earth" 2nd Edition, Princeton Univ. Press, Princeton, N.J., p. 310.

Gutenberg, B. and Richter, C., 1956. "Earthquake Magnitude, Intensity, Energy and Acceleration", 2, Bull. Seismol. Soc. Am., 46 (2), 105-143.

Hampel, A., 2002. The migration history of the Nazca Ridge along the Peruvian active margin: a re-evaluation. Earth and Planetary Science Letters.Volume 203, Issue 2, 30 October 2002, Pages 665–679
http://www.sciencedirect.com/science/article/pii/S0012821X02008592

Hsu, J.T., 1992. Quaternary uplift of the peuvian coast related to the subduction of the Nazca Ridge: 13.5 to 15.6 degrees south latitude. Quaternary International, Vol. 15-16, 1992, Pages 87-97.

Iida, K., D. Cox and G. Pararas-Carayannis, (1968). "Prelim. Catalogue of Tsunamis Occurring in the Pacific Ocean", Hawaii Institute of Geophysics, Univ. of Hawaii, Data Rept. No. 5.

Kikuchi, M. and Y. Yamanaga, 2001. Earthquake Information Center seismological note 105, Earthquake Information Center, Earthquake Research Institute, Univ. of Tokyo, 2001.

Lay, T., Ammon, C.J., Hutko, A.R. and H. Kanamori, 2010. Effects of Kinematic Constraints on Teleseismic Finite-Source Rupture Inversions: Great Peruvian Earthquakes of 23 June 2001 and 15 August 2007. Bulletin of the Seismological Society of America June 2010 v. 100 no. 3 p. 969-994.

Lomnitz, C., and Cabre' R. (1968). "The Peru Earthquake of October 17, 1966", Bull. Seism. Soc. Am., Vol. 58, No. 2, pp. 645-661, April.

Macharé and Ortlieb, 1992. Plio-Quaternary vertical motions and the subduction of the Nazca Ridge, central coast of Peru. Tectonophysics 205, 205, 97-108.

Melbourne, T. I., F. H. Webb, J.M. Stock, and C. Reigber, Rapid postseismic transients in subduction zones from continuous GPS, J. Geophys. Res., 107(B10), 2241, doi:10.1029/2001JB000555, 2002.

Nakano, H., 1923. Notes on the nature of the forces which give rise to the earthquake motions. Seismol. Bull. Central Meteorological Observatory Japan, 1, 92-122.

Okal, E. and Talandier, J.,1989. A variable-period mantle magnitude. Journal of Geophysical Research 94(B4): doi: 10.1029/88JB04010. issn: 0148-0227.

Okal, E. A., L. Dengler, S. Araya, J. C. Borrero, B. M. Gomer, S. Koshimura, G. Laos, D. Olcese, M. Ortiz , M. Swensson, V. V. Titov and F. Vegas, 2002. Field Survey of the Camaná, Perú Tsunami of 23 June 2001, Seismological Research Letters, November/December 2002, v. 73, p. 907-920

Ocola, L., 1966. "Earthquake Activity of Peru", Am. Geophys. U., Geophys. Monograph 10, 509-528.

Pararas-Carayannis, G, and A. S. Furumoto (1965). "Source Mechanism Study of the Alaska Earthquake and Tsunami of 27 March 1964, Part I, Water Waves", by G. Pararas-Carayannis; Part II. "Analysis of Raleigh Wave", by A. Furumoto, Rept. HIG65-17, 42 pp. Honolulu: Hawaii Inst. Geophys., Dec. 1965.

Pararas-Carayannis, G. (1968). "The Tsunami of October 17, 1966 in Peru", International Tsunami Information Center Newsletter, Vol. 1, No. 1, March 5.

Pararas-Carayannis, George 1969. Catalog of Tsunami in the Hawaiian Islands. World Data Center A-Tsunami

U.S. Dept. of Commerce Environmental Science Service Administration Coast and Geodetic Survey, May 1969.

Pararas-Carayannis, G., 1972. "The Great Alaska Earthquake of 1964 Source Mechanism of the Water Waves Produced", National Academy of Sciences - Committee on the Alaska Earthquake, Volume on Seismology and Geodesy, pp. 249-258.

Pararas-Carayannis, G., 1974. "An Investigation of Tsunami Source Mechanism off the Coast of Central Peru". Marine Geology, Vol. 17, pp. 235-247, Amsterdam: Elsevier Scientific Publishing Company. See also: http://drgeorgepc.com/Tsunami1966Peru.html

Pararas-Carayannis, George and Calebaugh P.J., 1977. Catalog of Tsunamis in Hawaii, Revised and Updated. World Data Center A – Tsunami report.

Pararas-Carayannis, G., 1996. The Earthquake and Tsunami of February 21, 1996 in Northern Peru. http://drgeorgepc.com/Tsunami1996Peru.html

Pararas-Carayannis, G., 2007. Earthquake and Tsunami of 15 August 2007 in Peru. http://www.drgeorgepc.com/Earthquake2007Peru.html

Pararas-Carayannis, G., 2010. Earthquake and Tsunami of 27 February 2010 in Chile - Evaluation of Source Mechanism and of Near and Far-field Tsunami Effects. Science of Tsunami Hazards", Vol. 29, No. 2, (2010)
http://www.drgeorgepc.com/Tsunami2010Chile.html

H. Perfettini, H., Avouac, J.P., and J.-C. Ruegg, 2005. Geodetic displacements and aftershocks following the 2001 *Mw* = 8.4 Peru earthquake: Implications for the mechanics of the earthquake cycle along subduction zones. JOURNAL OF GEOPHYSICAL RESEARCH, VOL. 110, B09404, 19 PP., 2005 doi:10.1029/2004JB003522.

Robinson, D.P., S. Das, S., and A. B. Watts, 2006. Earthquake Rupture Stalled by a Subducting Fracture Zone, Science 26 May 2006: Vol. 312 no. 5777 pp. 1203-1205

Rosenbauma G., Giles D., Saxon M., Betts P. G., Weinberg R. F., and C. Duboz, 2005A. Subduction of the Nazca Ridge and the Inca Plateau: Insights into the formation of ore deposits in Peru. Earth and Planetary Science Letters, Volume 239, Issues 1-2, 30 October 2005, Pages 18-3

Rosenbaum, G., Giles, D., Betts, P., Saxon, M., Weinberg, R., and C Duboz, 2005 B. American Geophysical Union, Fall Meeting 2005, abstract #T33B-0554,

Sacks I.S., 1983. The subduction of young lithosphere, J. Geophys. Res. 88 (1983) 3355-3366.

Sladen, A.; Madariaga, R.; Clévédé, E., 2004. Nonlinear Source Tomography Of The Mw=8.4, 23 June 2001 Arequipa, Peru Earthquake. *American Geophysical Union,Fall Meeting 2004, abstract #S53A-0181*

ISSN 8755-6839

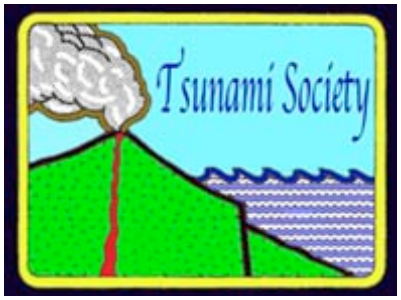

SCIENCE OF **TSUNAMI HAZARDS**

Journal of Tsunami Society International

Volume 31 **Number 2** **2012**

TSUNAMI SOCIETY INTERNATIONAL, 1741 Ala Moana Blvd. #70, Honolulu, HI 96815,USA.

WWW.TSUNAMISOCIETY.ORG